http://eprints.gla.ac.uk/171128/

Deposited on: 11 October 2018

Fractional elastoplastic constitutive model for soils based on a novel 3D fractional plastic flow rule

De-chun LU[1]; Jing-yu LIANG[2], Xiu-li DU[3]*, Chao MA[4], Zhi-wei GAO[5]

ABSTRACT:

A novel three-dimensional (3D) fractional plastic flow rule that is not limited by the coordinate basis of the differentiable function is proposed based on the fractional derivative and the coordinate transformation. By introducing the 3D fractional plastic flow rule into the characteristic stress space, a 3D fractional elastoplastic model for soil is established for the first time. Only five material parameters with clear physical significance are required in the proposed model. The capability of the model in capturing the strength and deformation behaviour of soils under true 3D stress conditions is verified by comparing model predictions with test results.

Keywords: Soils, Constitutive model, Fractional plastic flow rule, True 3D stress condition, Critical state, Characteristic stress.

[1]Ph.D., Professor. Key Laboratory of Urban Security and Disaster Engineering of Ministry of Education, Beijing University of Technology, Beijing, 100124, China. E-mail: dechun@bjut.edu.cn.

[2] Ph.D., Candidate. Key Laboratory of Urban Security and Disaster Engineering of Ministry of Education, Beijing University of Technology, Beijing, 100124, China. E-mail: liangjingyuy@163.com.

[3]* Ph.D., Professor. Key Laboratory of Urban Security and Disaster Engineering of Ministry of Education, Beijing University of Technology, Beijing, 100124, China (Corresponding author). E-mail: duxiuli5@126.com.

[4] Ph.D., Beijing Advanced Innovation Center for Future Urban Design, Beijing University of Civil Engineering and Architecture, Beijing, 102616, China. E-mail: machao@bucea.edu.cn.

[5] Ph.D., School of Engineering, University of Glasgow, Glasgow, G12 8LT, UK. E-mail: zhiwei.gao@glasgow.ac.uk.

1   Introduction

30   Fractional derivative can generalise integer derivatives to all real (and even complex) orders,

31   and thus provides a way to extend the gradient into the fractional gradient. In contrast to the gradient,

32   the fractional gradient is not orthogonal with the surface of the differentiable function. The ability

33   of the fractional derivative to adjust gradient direction was utilized by Sumelka (2014) to describe

34   the direction of the viscoplastic strain increments, and thus the concept of the fractional plastic flow

35   rule was originally proposed (Sumelka, 2014; Sumelka and Nowak, 2016). The plastic strain

36   increment direction can be obtained by the fractional partial derivative of the yield function with

37   respect to the Cauchy's stress. However, in order to obtain the explicit solutions of the fractional

38   derivative of the yield function, the yield function has to be directly expressed in terms of the

39   principal stresses (Sumelka, 2014) or the stress components (Sumelka and Nowak, 2016), because

40   the chain rule with the same fractional order for the fractional partial derivative does not work. The

41   performance of the fractional plastic flow rule in modelling mechanical behaviour of granular soils

42   in triaxial compression condition has been explored by Sun and Xiao (2017). A series of fractional

43   order plastic models have been established (Sun and Xiao, 2017; Sun et $al.$, 2017) by combining the

44   fractional plastic flow rule with plastic modulus in existing models (Li and Dafalias, 2000; Xiao et

45   $al.$, 2004) to describe stress-dilatancy and strain hardening/softening of granular soils. Furthermore,

46   Sun et $al.$ (2018a; 2018b) originally used the current stress state in the definition of the fractional

47   derivative to model the state-dependent behaviour of granular soils. However, the fractional plastic

48   flow rule adopted in these models were all derived by the fractional derivative of the yield function

49   with respect to two stress invariants, i.e., the mean stress p and the deviatoric stress q under triaxial

50   compression conditions, rather than the general stress tensor. The existing fractional elastoplastic

51   models for soils suits only for triaxial compression conditions, and the strength and deformation

52   behaviour of soils under true 3D stress conditions has not been described. Indeed, the application of

53   the fractional derivative in elastoplastic constitutive modelling for soils is still at the very beginning.

54   A 3D yield function and the fractional plastic flow rule, which should be matched, are essential

55   for establishing a 3D fractional constitutive model for soils. Up to the present, a yield function in

56   the 3D stress space can be constructed using two methods: (i) Direct method in which the yield

57   function is explicitly expressed in terms of the stress components (Borja et $al.$, 2003; Khalili and

58   Liu, 2008; Duriez and Vincens, 2015; Panteghini and Lagioia, 2018); (ii) Indirect method where the

59 yield function is constructed under triaxial compression conditions in a transitional space, which

60 can reflect yield properties of soils under true 3D stress conditions (Chowdhury and Nakai, 1998;

61 Collins, 2003; Yao $et\ al.$, 2009; Ma $et\ al.$, 2017). However, by applying the existing fractional flow

62 rule (Sumelka, 2014) to the commonly used 3D yield functions constructed by the above methods,

63 explicit expressions of the fractional derivative with respect to general stress components σ_{ij} cannot

64 be obtained. Thus, a 3D fractional plastic flow rule with no limitation of the coordinate basis of the

65 yield function is eagerly needed for establishing 3D fractional plasticity model.

66   In this paper, a novel 3D fractional plastic flow rule that can well match the classical plasticity

67 theory is presented based on the covariant transformation. Furthermore, the characteristic stress (Lu

68 $et\ al.$, 2017; Ma $et\ al.$, 2017) is introduced to describe the mechanical behaviours of soil under true

69 3D stress conditions. The combination of the new 3D fractional plastic flow rule and the

70 characteristic stress presents a new approach to establishing a 3D fractional elastoplastic constitutive

71 model. The strength and deformation behaviour of soils under true 3D stress conditions can thus be

72 directly described.

73 ## 2   A novel 3D fractional plastic flow rule

74   The plastic flow rule in classical plasticity theory is used to determine the direction of the

75 plastic strain increment. The plastic strain increment direction is usually determined by the

76 orthogonality with respect to the plastic potential surface. If the plastic potential function is chosen

77 to be identical to the yield function, the associated flow rule is adopted (Wood, 1990; Sun $et\ al.$,

78 2004; Yao $et\ al.$, 2009; Zhou and Sheng, 2015). However, the associated flow rule does not work

79 for most geomaterials (Lade $et\ al.$, 1987; Collins and Houlsby, 1997). Therefore, the non-associated

80 flow rule is usually used (Lu $et\ al.$, 2016; Gao and Zhao, 2017). There are two approaches to

81 obtaining the desired plastic strain increment direction **n**: (i) constructing a plastic potential function

82 g to determine **n** by orthogonality as shown in Fig. 1(a); (ii) determining **n** based on an existing

83 yield function f in a non-orthogonal way as shown in Fig. 1(b).

84

85   (a)   (b)

86 Fig. 1 Two approaches to determining the plastic strain increment direction:

87 (a) orthogonal way; (b) non-orthogonal way.

88

89   However, the plastic potential function may be difficult to construct in a simple way and

90   additional parameters could be required. The fractional partial derivative poses the ability to adjust

91   the gradient direction based on an existing function in a non-orthogonal way. Moreover, the yield

92   curve is necessary for the plastic theory. Therefore, fractional partial derivatives of the yield function

93   is a proper option as the non-orthogonal way for determining the plastic strain increment direction

94   (Sumelka and Nowak, 2016; Sun and Xiao, 2017).

95   **2.1   Fractional derivative**

96   There are three widely used definitions for fractional derivatives, i.e., Grünwald-Letnikov,

97   Riemann-Liouville, and Caputo definition (Podlubny, 1998; Mashayekhi *et al.*, 2018). Among them,

98   the Caputo derivative has the weak singularity and the Caputo derivative of a constant is 0, making

99   it the widely used one (Podlubny, 1998; Meng *et al.*, 2016; Colinas-Armijo *et al.*, 2016;). The

100   Caputo derivative used in this paper is expressed as:

101
$$
{}_{a}^{C}D_{x}^{\mu}f(x)=\frac{1}{\Gamma(n-\mu)}\int_{a}^{x}\frac{f^{(n)}(\tau)}{(x-\tau)^{\mu+1-n}}\mathrm{d}\tau,\ \ (x>a) \tag{1}
$$

102   where $^{C}D^{\mu}$ means the Caputo derivative of order μ. a is the starting point of integral, which is chosen

103   as 0 in this paper. x is the independent variable, which is used to express the current stress state in

104   this paper. n is the smallest integer greater than μ, $n=[\mu]+1$, where $[\cdot]$ denotes the floor function. $n=1$

105   when $0<\mu\leq1$. $\Gamma(\cdot)$ is Euler Gamma function, which is expressed as $\Gamma(z)=\int_{0}^{\infty}e^{-\tau}\tau^{z-1}\mathrm{d}\tau$, the real

106   part of z is larger than 0, i.e., $\mathrm{Re}(z)>0$. The explicit expression of the Caputo derivative of a

107   power function $f(x)=x^{m}$ can be obtained as follows:

108
$$
{}_{0}^{C}D_{x}^{\mu}(x^{m})=\frac{\partial^{\mu}(x^{m})}{\partial x^{\mu}}=\frac{\Gamma(m+1)}{\Gamma(m+1-\mu)}x^{m-\mu} \tag{2}
$$

109   where the exponent m (>-1) is restricted by the integrability of $f(x)$.

110   When the fractional derivative is used to get the partial derivatives of a function, the fractional

111   gradient can be obtained and it is flexible to adjust the flow direction by adjusting the fractional

112   order μ. This is exactly what is desired for the non-orthogonal way mentioned above to determine

113   the plastic strain increment direction.

114   **2.2   A 3D fractional plastic flow rule**

115   In the classical plastic theory, the plastic strain increment direction is determined by the

116 gradient of the plastic potential function g. The plastic strain increment is expressed as follows:

$$d\varepsilon_{ij}^{p} = d\lambda \frac{\partial g}{\partial \sigma_{ij}} \tag{3}$$

118 where $d\lambda$ is the plastic multiplier for general plastic flow rule, and $\partial g/\partial \sigma_{ij}$ is the gradient of the

119 plastic potential function, respectively. The plastic potential function can be constructed using the

120 principal stresses σ_i (i=1, 2, 3), which is expressed as $g(\sigma_i)$. The gradient direction of $g(\sigma_i)$ in the σ_i

121 coordinate system is thus expressed by $n_i^{(\sigma)} = \partial g/\partial \sigma_i$. The plastic potential function of soils can

122 also be constructed by any set of stress variables S_k (k=1, 2, 3), where S_k is a function of σ_i, i.e.,

123 $S_k(\sigma_i)$. The plastic potential function can be expressed as $g(S_k)$ in the S_k coordinate system, and its

124 gradient direction is $n_k^{(S)} = \partial g/\partial S_k$. Here, $n_k^{(S)}$ and $n_i^{(\sigma)}$ are components of the gradient vector **n**

125 in the S_k and σ_i coordinate systems, respectively, as shown in Fig. 2. Therefore, a covariant

126 transformation coefficient l_i^k is needed to transform the components of the vector **n** in the S_k

127 coordinate system into the σ_i coordinate system. l_i^k is the partial derivative of S_k with respect to σ_i,

128 and is expressed as follows:

$$l_i^k = \frac{\partial S_k}{\partial \sigma_i} \tag{4}$$

130

131 Fig. 2 Coordinate transformation of the plastic strain increment direction

132 Therefore, according to the covariant transformation rule, $n_i^{(\sigma)}$ in the σ_i coordinate system can be

133 expressed in terms of $n_k^{(S)}$ in the S_k coordinate system.

$$n_i^{(\sigma)} = n_k^{(S)} l_i^k = n_k^{(S)} \frac{\partial S_k}{\partial \sigma_i} \tag{5}$$

135 where S_k is an interim coordinate system for specific purposes, like the Cartesian rectangular

136 coordinate system, the cylindrical coordinate system or the spherical coordinate system etc. The

137 commonly used stress invariants p, q and θ or other stress invariants, like I_1, I_2 and I_3, are specific

138 examples of S_k. Generally, the components of the gradient vector of g can be expressed as

139 $n_{kl}^{(S)} = \partial g/\partial S_{kl}$ in the S_{kl} space and $n_{ij}^{(\sigma)} = \partial g/\partial \sigma_{ij}$ in the σ_{ij} space, respectively. Therefore, the

140 general covariant transformation between $n_{kl}^{(S)}$ and $n_{ij}^{(\sigma)}$ can be accomplished by the covariant

141 transformation coefficient $l_i^k l_j^l = \partial S_{kl}/\partial \sigma_{ij}$ as follows:

5

142
$$n_{ij}^{(\sigma)} = n_{kl}^{(S)} l_i^k l_j^l = n_{kl}^{(S)} \frac{\partial S_{kl}}{\partial \sigma_{ij}} \tag{6}$$

143   For geomaterials, stress invariants p, q and θ are usually adopted to establish constitutive

144   models (Mortara, 2015). The corresponding strain increment $\left(d\varepsilon_v^p, d\varepsilon_s^p, d\varepsilon_\theta^p \right)$ can be obtained as

145   follows:

146
$$\left(d\varepsilon_v^p, d\varepsilon_s^p, d\varepsilon_\theta^p \right) = d\lambda \left(n_p, n_q, n_\theta \right) \tag{7}$$

147   where $(n_p, n_q, n_\theta) = (\partial g/\partial p, \partial g/\partial q, \partial g/\partial \theta)$ represents the plastic strain increment direction. Two

148   orthogonal planes, i.e., the meridian plane and the deviatoric plane, are used to analyse

149   characteristics of models (Khalili and Liu, 2008; Yao $et~al.$, 2009; Lu $et~al.$, 2018). The current stress

150   state point A can thus be represented in the meridian plane with the stress Lode angle θ (θ is

151   equivalent to the intermediated principal stress coefficient b, namely, $b = 2\tan\theta / (\sqrt{3} + \tan\theta)$) and

152   in the deviatoric plane with $p=p_A$, as shown in Fig. 3(a) and (b), respectively. The plastic strain

153   increment direction of point A can also be divided into two components: the vector $\mathbf{n_{mg}}=(n_p, n_q)$ in

154   the meridian plane and the vector $\mathbf{n_{dg}}=(n_q, n_\theta)$ in the deviatoric plane, which are orthogonal to the

155   plastic potential curves as shown in Fig. 3 (a) and (b), respectively. Further, the obtained plastic

156   strain increment direction in the (p, q, θ) coordinate system can be transformed into the σ_{ij} space.

157   The transformation is accomplished by $\partial p/\partial \sigma_{ij}$, $\partial q/\partial \sigma_{ij}$ and $\partial \theta/\partial \sigma_{ij}$, which is a common practice in

158   the classical elastoplastic theory as follows:

159
$$d\varepsilon_{ij}^p = d\lambda \left(n_p \frac{\partial p}{\partial \sigma_{ij}} + n_q \frac{\partial q}{\partial \sigma_{ij}} + n_\theta \frac{\partial \theta}{\partial \sigma_{ij}} \right) \tag{8}$$

160

161   (a)   (b)

162   Fig. 3 Plastic strain increment direction in: (a) the meridian plane with $\theta=\theta_A$; (b) the deviatoric plane

163   with $p=p_A$.

164   The fractional derivative can thus be a new tool and a proper approach to extending the classical

165   plastic flow rule. Sumelka (2014) proposed a concept of fractional plastic flow rule and used it as a

166   new tool to introduce material heterogeneity/multi-scale effects into the constitutive model.

167
$$d\varepsilon_{ij}^p = \Lambda \frac{\partial^\mu f}{\partial \sigma_{ij}{}^\mu} \tag{9}$$

168   where Λ is the plastic multiplier for the fractional plastic flow rule. $\partial^{\mu} f / \partial \sigma_{ij}{}^{\mu}$ is fractional plastic

169   strain increment direction which is represented by the fractional partial derivative of the yield

170   function f with respective to σ_{ij}. The flow rule becomes associated when μ=1. However, the explicit

171   expression of the flow direction in the 3D stress space determined by Eq. (9) can only be derived

172   by the yield function directly expressed by σ_{ij}, such as the Huber-Mises-Hencky yield function

173   (Sumelka, 2014; Sumelka and Nowak, 2016). For geomaterials, the yield function f is usually and

174   more conveniently expressed in terms of the stress invariants p, q and θ or other stress components

175   for true 3D stress conditions. That is, the constraint of Eq. (9) on the coordinate basis of the yield

176   function limits the application of the fractional plastic flow rule in the form of Eq. (9).

177   A novel fractional plastic flow rule that suitable for the true 3D stress conditions can be

178   established based on the view of the coordinate transformation rather the chain rule with the same

179   fractional order for the fractional derivative. The proposed fractional plastic flow rule is not limited

180   by the coordinate basis of the yield function and can be obtained in two steps:

181   (*i*) Determine the plastic strain increment direction $m_{kl}^{(S)}$ in the S_{kl} space by the fractional

182   partial derivative of the yield function with respect to S_{kl}. Therefore, the components of the plastic

183   strain increment can be determined in the S_{kl} space as follows:

184
$$\mathrm{d}\varepsilon_{kl}^{\mathrm{p}(S)} = \Lambda m_{kl}^{(S)} = \Lambda \frac{\partial^{\mu} f}{\partial S_{kl}{}^{\mu}} \tag{10}$$

185   (*ii*) Transform the determined plastic strain components in the S_{kl} space into the σ_{ij} space by the

186   covariant transformation coefficient $l_i^k l_j^l = \partial S_{kl} / \partial \sigma_{ij}$. Eventually, a novel 3D fractional plastic flow

187   rule in the σ_{ij} space is obtained as follows:

188
$$\mathrm{d}\varepsilon_{ij}^{\mathrm{p}(\sigma)} = l_i^k l_j^l \mathrm{d}\varepsilon_{kl}^{\mathrm{p}(S)} = \Lambda \frac{\partial^{\mu} f}{\partial S_{kl}{}^{\mu}} \frac{\partial S_{kl}}{\partial \sigma_{ij}} \tag{11}$$

189   It is crucial to transform the determined plastic strain increment direction into the σ_{ij} space.

190   Based on the proposed fractional plastic flow rule Eq. (11), the general form of the plastic strain

191   increments under the true 3D stress conditions can be expressed by the stress tensor σ_{ij}, which are

192   actually essential for soil property analysis and model application. That is, the general form of the

193   fractional plastic flow rule is essential and make it possible to establish a 3D fractional constitutive

194   model for geomaterials in the framework of the plastic theory.

195   For the yield function constructed by the stress invariants S_k in the S_{kl} space, the 3D fractional

196   plastic flow rule can be written as:

$$\mathrm{d}\varepsilon_{ij}^{\mathrm{p}} = \Lambda \frac{\partial^{\mu} f}{\partial S_k{}^{\mu}} \frac{\partial S_k}{\partial \sigma_{ij}} \tag{12}$$

198   where $\partial^{\mu} f / \partial S_k{}^{\mu}$ is the determined plastic strain increment direction in the S_k coordinate system,

199   which can be transformed into the σ_{ij} space by $\partial S_k / \partial \sigma_{ij}$. When the commonly used stress invariants

200   p, q and θ are chosen to construct the yield function, the 3D fractional plastic flow rule becomes:

$$\mathrm{d}\varepsilon_{ij}^{\mathrm{p}} = \Lambda \left(m_p \frac{\partial p}{\partial \sigma_{ij}} + m_q \frac{\partial q}{\partial \sigma_{ij}} + m_{\theta} \frac{\partial \theta}{\partial \sigma_{ij}} \right) \tag{13}$$

202   The plastic strain increment direction is thus first expressed by $(m_p, m_q, m_{\theta})=(\partial^{\mu} f / \partial p^{\mu}$,

203      $\partial^{\mu} f / \partial q^{\mu}$, $\partial^{\mu} f / \partial \theta^{\mu}$) in the (p, q, θ) coordinate system, and then transformed into the σ_{ij} space by

204      $\partial p / \partial \sigma_{ij}$, $\partial q / \partial \sigma_{ij}$ and $\partial \theta / \partial \sigma_{ij}$. The plastic strain increment direction represented by (m_p, m_q, m_{θ}) can be

205   divided into two components $\mathbf{m_{m\mu}}=(m_p, m_q)$ and $\mathbf{m_{d\mu}}=(m_q, m_{\theta})$ in two orthogonal planes, i.e., the

206   meridian plane and the deviatoric plane. $\mathbf{m_{m\mu}}$ and $\mathbf{m_{d\mu}}$ are represented by the red solid arrows, as

207   shown in Fig. 4. When $\mu=1$, the fractional gradient directions degenerate to the normal direction of

208   the yield curve, which can be decomposed into $\mathbf{n_{m f}}$ and $\mathbf{n_{d f}}$, indicated by the blue solid arrows. The

209   deviation degree of the fractional gradient direction from the normal of the yield curve can be

210   adjusted by μ.

211   In particular, when the yield function is expressed only by q and θ and is independent of p for

212   the hydrostatic pressure independent materials, the yield curve in the meridian plane is a straight

213   line that is parallel to the p-axis, as shown in Fig. 4(c). Therefore, the fractional derivative of f with

214   respect to p is 0 and is independent of μ. The plastic strain increment direction becomes $(0, m_q, m_{\theta})$.

215      $\mathbf{m_{m\mu}}$ is perpendicular to the yield line in the meridian plane. Nonetheless, $\mathbf{m_{d\mu}}$ still depends on μ,

216   which is similar to the effects of μ on $\mathbf{m_{d\mu}}$ in Fig. 4(b). When the yield function is expressed only

217   by p and q and is independent of θ, the yield curve in the deviatoric plane is a circle as shown in

218   Fig. 4(d). Then the fractional derivative of f with respect to θ is 0 and is independent of μ. The plastic

219   strain increment direction can be represented by $(m_p, m_q, 0)$. $\mathbf{m_{d\mu}}$ is perpendicular to the yield circle

220   in the deviatoric plane. However, $\mathbf{m_{m\mu}}$ still depends on μ, which is similar to the effects of μ on $\mathbf{m_{m\mu}}$

221   in Fig. 4(a).

222

223   (a)   (b)   (c)   (d)

224   Fig. 4 Fractional plastic strain increment direction with the yield function constructed:

225   (a) by p, q and θ in the meridian plane; (b) by p, q and θ in the deviatoric plane;

226   (c) only by q and θ in the meridian plane; (d) only by p and q in the deviatoric plane.

227

228   The proposed 3D fractional plastic flow rule offers a new approach to determine the plastic

229   strain increment directions under true 3D stress conditions. Therefore, a new possibility is provided

230   for establishing true 3D fractional elastoplastic constitutive model for soils.

3   A 3D fractional elastoplastic model in the characteristic stress space

232   In order to describe soil behaviour under true 3D stress conditions in a simple way, some

233   specialized stress concepts were proposed, like the t_{ij} stress (Chowdhury and Nakai, 1998, Nakai *et*

234   *al.*, 2011), the transformed stress (Yao *et al.*, 2004; Sun *et al.*, 2004; Yao *et al.*, 2009) and the

235   characteristic stress (Lu *et al.*, 2017; Ma *et al.*, 2017) etc. The yield function $\hat{f}$ can be constructed

236   using only two common stress invariants $\hat{p}$ and $\hat{q}$ in a chosen specialized stress space, which is

237   able to directly describe soil behaviour under true 3D stress conditions. That is, the 3D constitutive

238   model can be directly established under triaxial compression conditions in the specialized stress

239   space. The new proposed fractional plastic flow rule becomes simpler and more powerful by

240   combining with a specialized stress space, and Eq. (13) becomes:

$$d\varepsilon_{ij}^{p} = \Lambda \left(\frac{\partial^{\mu}\hat{f}}{\partial\hat{p}^{\mu}} \frac{\partial\hat{p}}{\partial\hat{\sigma}_{ij}} + \frac{\partial^{\mu}\hat{f}}{\partial\hat{q}^{\mu}} \frac{\partial\hat{q}}{\partial\hat{\sigma}_{ij}} \right) \tag{14}$$

242   The characteristic stress space is a proper choice to describe the soil behaviour especially for

243   the true 3D stress conditions (Lu *et al.*, 2017; Ma *et al.*, 2017). The combination of the characteristic

244   stress and the fractional derivative is elaborately attempted and discussed in this paper.

3.1   Characteristic stress

246   The concept of the characteristic stress, which was originally proposed by Lu *et al.* (2017)

247   presents a new approach to describing the soil behaviour under true 3D stress conditions (Ma *et al.*,

248   2017). The principal values of σ_{ij} that is denoted by $\hat{\sigma}_{mn}$ (m, n=1, 2, 3) can be obtained by the

249   coordinate transformation (Chowdhury and Nakai, 1998) in the σ_{ij} space as follows:

250 $$\hat{\sigma}_{mn} = Q_{mi}Q_{nj}\sigma_{ij} = \begin{cases} \sigma_m & m = n \\ 0 & m \neq n \end{cases} \tag{15}$$

251 where Q_{ij} is an orthogonal tensor which transforms the general stress tensor to its principal values.

252 The principal stress tensor of the characteristic stress in this paper can be expressed by the following

253 equation:

254 $$\hat{c}_{mn} = \begin{cases} p_r\left(\dfrac{\sigma_m}{p_r}\right)^{\beta} & m = n \\ 0 & m \neq n \end{cases} \tag{16}$$

255 where p_r is the reference stress for dimensionless transformation, and $p_r=1\text{kPa}$ is usually used. β is

256 a material parameter and varies from 0 to 1 for different geomaterials. The characteristic principal

257 stress is coaxial with the general principal stress. Finally, the characteristic stress tensor can be

258 obtained by the following coordinate transformation in the c_{ij} space:

259 $$c_{ij} = Q_{im}Q_{jn}\hat{c}_{mn} \tag{17}$$

260 The comparison of stress variables in the σ_{ij} space and the c_{ij} space is listed in Tab. 1, in which φ_c is

261 the internal frictional angel under triaxial compression conditions.

262 Tab. 1 Comparison of stress variables in the general stress space and the characteristic stress space

	General stress space	Characteristic stress space
Stress tensor	σ_{ij}	c_{ij}
Principal stress	$\sigma_i,\ \ i=1,2,3$	$c_i = p_r\left(\dfrac{\sigma_i}{p_r}\right)^{\beta},\ \ i=1,2,3$
Mean stress	$p=\sigma_{ij}\delta_{ij}/3$	$c_\text{n}=c_{ij}\delta_{ij}/3$
Deviatoric stress	$q = \sqrt{\dfrac{3}{2}\left(\sigma_{ij}-p\delta_{ij}\right)\left(\sigma_{ij}-p\delta_{ij}\right)}$	$c_\text{s} = \sqrt{\dfrac{3}{2}\left(c_{ij}-c_\text{n}\delta_{ij}\right)\left(c_{ij}-c_\text{n}\delta_{ij}\right)}$
Stress ratio	$\eta=q/p$	$\chi=c_\text{s}/c_\text{n}$
Critical stress ratio	$M = \dfrac{6\sin\varphi_c}{3-\sin\varphi_c}$	$F = 3\dfrac{\left(1+\sin\varphi_c\right)^{\beta}-\left(1-\sin\varphi_c\right)^{\beta}}{\left(1+\sin\varphi_c\right)^{\beta}+2\left(1-\sin\varphi_c\right)^{\beta}}$

263 **3.2   Fractional plastic model in characteristic stress space**

264   Three essential parts for developing a fractional plastic model, including the yield function, the

265 fractional plastic flow rule and the hardening parameter, are all established in the characteristic stress

266 space. Among them, the combination of the proposed fractional plastic flow rule and the

267 characteristic stress is used to capture the plastic deformation properties of soils under true 3D stress

268 conditions.

269 *3.2.1 Yield function*

270   For the sake of simplicity, the yield function established in the characteristic stress space takes

271 the form of an ellipsoid. It has the same form and convexity with the yield function of the modified

272 Cam-clay (MCC) model (Roscoe and Burland, 1968). The yield function in this paper can be

273 expressed as:

274
$$f = c_s^2 + N^2 \left(c_n^2 - c_{nx}c_n \right) = 0 \tag{18}$$

275 where N is the ratio of the vertical axis and the horizontal axis of the elliptic yield curve as shown

276 in Fig. 5, which is the geometrical role of M in the yield function of the MCC model. The failure

277 stress ratio F is the physical role of M in the MCC model for describing the critical state of soil. N

278 and F equal to M when $\beta=1$. The equivalent consolidation pressure c_{nx} is the intersection coordinate

279 of the yield curve with the abscissa and can be expressed as Eq. (19). The role of c_{nx} is to connect

280 the yield curve with the hardening rule, which is described in section 3.2.3.

281
$$c_{nx} = \frac{c_s^2 + N^2 c_n^2}{N^2 c_n} \tag{19}$$

282

283 Fig. 5 Yield surface in the meridian plane

284

285   Only two stress invariants c_n and c_s are used to construct the yield function. Thus, the yield

286 surface in the c_{ij} space shown in Fig. 6(a) is an axially symmetric ellipsoid with respect to the c_n-

287 axis. However, the corresponding yield surface in the σ_{ij} space is an irregular, smooth and convex

288 three-axis symmetric surface when $0<\beta<1$ as shown in Fig. 6(b).

289

290   (a)   (b)

291 Fig. 6 Yield surface: (a) in the c_{ij} space; (b) in the σ_{ij} space.

292

293   Fig. 7 shows the yield curves in the meridian plane and the deviatoric plane of the σ_{ij} space.

294 All the yield curves pass through the critical state point (p_0, $M \cdot p_0$). For a certain value of β ($0<\beta<1$),

295 yield curve is asymmetric with respect to the *p*-axis in the meridian plane as shown in Fig. 7(a) and

296 is a curved triangle in the deviatoric plane as shown in Fig. 7(b). The value of β reflects effects of

297 Lode angle θ or the intermediate principal stress coefficient *b* on soil behaviour. The yield curves of

298 β=0.1 and β=0.01 are almost coincident, thus β=0.1 can be taken as the approximate lower bound

299 in this paper for saving the computational cost. As *q* increases to the critical state along the stress

300 path of constant p_0 under the monotonic loading, the yield curve of β=0.1 in the meridian plane

301 gradually evolves and expands, as shown in Fig. 8(a). The yield curve in the deviatoric plane

302 changes from an approximate circle to a curved triangle, as shown in Fig. 8(b), which reflects the

303 stress-induced anisotropy of geomaterials.

304

305 (a)   (b)

306 Fig. 7 Yield curves in the σ_{ij} space with the decrease of β:

307 (a) in the meridian plane; (b) in the deviatoric plane.

308

309 (a)   (b)

310 Fig. 8 Yield curve in the σ_{ij} space with the increase of *q* at a constant *p*:

311 (a) in the meridian plane; (b) in the deviatoric plane.

312

313 *3.2.2 Fractional plastic flow rule*

314   The fractional plastic flow rule and the characteristic stress are independent in definition but

315 complementary in property description: one for adjusting the plastic strain increment direction, and

316 the other for describing the soil behaviour under true 3D stress conditions in a simple and unified

317 way. By introducing the new proposed fractional plastic flow rule into the characteristic stress space,

318 a novel sight to describe the soil behaviour is proposed. The fractional plastic flow rule in the

319 characteristic stress space is thus established by referring Eq. (14) as follows:

320
$$\mathrm{d}\varepsilon_{ij}^{\mathrm{p}} = \Lambda \left(\frac{\partial^{\mu} f}{\partial c_{\mathrm{n}}{}^{\mu}} \frac{\partial c_{\mathrm{n}}}{\partial c_{ij}} + \frac{\partial^{\mu} f}{\partial c_{\mathrm{s}}{}^{\mu}} \frac{\partial c_{\mathrm{s}}}{\partial c_{ij}} \right) \tag{20}$$

321 where the fractional partial derivative of the yield function (i.e., Eq. (18)) with respect to c_{n} and c_{s}

322 are determined as follows:

323

$$\begin{cases} \dfrac{\partial^{\mu} f}{\partial c_{\mathrm{n}}{}^{\mu}} = \dfrac{2N^2 c_{\mathrm{n}}^{2-\mu}}{\Gamma(3-\mu)} - \dfrac{N^2 c_{\mathrm{n}x} c_{\mathrm{n}}^{1-\mu}}{\Gamma(2-\mu)} \\ \dfrac{\partial^{\mu} f}{\partial c_{\mathrm{s}}{}^{\mu}} = \dfrac{2c_{\mathrm{s}}^{2-\mu}}{\Gamma(3-\mu)} \end{cases} \tag{21}$$

Introducing $c_{\mathrm{n}x}$ expressed by Eq. (19) and the recursive property of gamma function, i.e.,

$\Gamma(x+1)=x\cdot\Gamma(x)$ into Eq. (21) yields:

326

$$\begin{cases} \dfrac{\partial^{\mu} f}{\partial c_{\mathrm{n}}{}^{\mu}} = \dfrac{\mu N^2 c_{\mathrm{n}}^2 - (2-\mu)c_{\mathrm{s}}^2}{\Gamma(3-\mu)c_{\mathrm{n}}^{\mu}} \\ \dfrac{\partial^{\mu} f}{\partial c_{\mathrm{s}}{}^{\mu}} = \dfrac{2c_{\mathrm{s}}^{2-\mu}}{\Gamma(3-\mu)} \end{cases} \tag{22}$$

The covariant transformation coefficient, i.e., the partial differential of c_{n} and c_{s} with respect to c_{ij},

can be derived as follows:

329

$$\begin{cases} \dfrac{\partial c_{\mathrm{n}}}{\partial c_{ij}} = \dfrac{1}{3}\delta_{ij} \\ \dfrac{\partial c_{\mathrm{s}}}{\partial c_{ij}} = \dfrac{3(c_{ij} - c_{\mathrm{n}}\delta_{ij})}{2c_{\mathrm{s}}} \end{cases} \tag{23}$$

By substituting Eqs. (22) and (23) into Eq. (20), the plastic strain increment can be expressed as:

331

$$\mathrm{d}\varepsilon_{ij}^{\mathrm{p}} = \Lambda \left[\frac{\mu N^2 c_{\mathrm{n}}^2 - (2-\mu)c_{\mathrm{s}}^2}{\Gamma(3-\mu)c_{\mathrm{n}}^{\mu}} \frac{1}{3}\delta_{ij} + \frac{2c_{\mathrm{s}}^{2-\mu}}{\Gamma(3-\mu)} \frac{3(c_{ij} - c_{\mathrm{n}}\delta_{ij})}{2c_{\mathrm{s}}} \right] \tag{24}$$

The ratio of the plastic volumetric strain increment $\mathrm{d}\varepsilon_{\mathrm{v}}^{\mathrm{p}}$ to the plastic deviatoric strain

increment $\mathrm{d}\varepsilon_{\mathrm{s}}^{\mathrm{p}}$ (i.e., the stress-dilatancy ratio $d = \mathrm{d}\varepsilon_{\mathrm{v}}^{\mathrm{p}}/\mathrm{d}\varepsilon_{\mathrm{s}}^{\mathrm{p}}$) can thus be obtained from Eq. (20)

together with Eq. (22). The stress-dilatancy ratio d is the reflection of the plastic strain

direction, which can be expressed as follows.

336

$$d = \frac{\mathrm{d}\varepsilon_{\mathrm{v}}^{\mathrm{p}}}{\mathrm{d}\varepsilon_{\mathrm{s}}^{\mathrm{p}}} = \frac{\Lambda \cdot \dfrac{\partial^{\mu} f}{\partial c_{\mathrm{n}}{}^{\mu}}}{\Lambda \cdot \dfrac{\partial^{\mu} f}{\partial c_{\mathrm{s}}{}^{\mu}}} = \frac{\mu N^2 - (2-\mu)\chi^2}{2\chi^{2-\mu}} \tag{25}$$

The condition of $\varphi_{\mathrm{c}}=30°$ and $\beta=0.4$ is taken as a special case for demonstration, and $N=0.769$

and $\mu=0.537$ can be determined by methods in the following section 3.3.3. When the soil is loaded

from the isotropic compression point A_0 to the point A_1 along the conventional triaxial compression

path A_0A_{f}, the yield curve and the plastic strain increment directions are shown in Fig. 9. As shown

in Fig. 9(a), the yield curve in the meridian plane through the current stress point A_1 is indicated by

13

342 the black ellipsoidal curve. The plastic strain increment directions on the yield curve for μ=0.537

343 are indicated by the red solid arrow. The normal gradient directions when μ=1 are orthogonal to the

344 yield curve, and is indicated by the blue dash arrow. Since the expression of the yield function is

345 independent of θ, the yield curve in the deviatoric plane is a circle as shown in Fig. 9(b). Therefore,

346 the plastic strain increment direction is perpendicular to the yield circle in the deviatoric plane and

347 independent of μ. The overview of the yield surface and the plastic strain increment directions in

348 the c_{ij} space are shown in Fig. 10.

349

350   (a)   (b)

351   Fig. 9 Plastic strain increment direction in the c_{ij} space at the current loading point:

352   (a) in the meridian plane with $\theta=\theta_A$; (b) in the deviatoric plane with $p=p_A$.

353

354   Fig. 10 Plastic strain increment direction in the c_{ij} space.

355

356   For the condition of μ=0.537, the variation rules of the plastic strain increments with increasing

357 χ are shown in Fig. 11. When χ=0, the plastic strain increment direction is horizontal to the right and

358 is independent of μ, which means that plastic deviatoric strain does not occur under the isotropic

359 compression conditions, i.e., $d\varepsilon_s^p = 0$. With the increase of χ, the plastic strain increment directions

360 gradually change from horizontal to vertical, and $d\varepsilon_v^p > 0$. When χ reaches F, the stress state

361 reaches the critical state, but not the peak of the yield curve. The plastic strain increment direction

362 is vertically upward, which means that plastic volumetric strain does not occur, i.e., $d\varepsilon_v^p = 0$. It

363 should be noticed that for a fixed value of χ, the plastic strain increment directions on different yield

364 curves are the same, as shown in Fig. 11.

365

366   Fig. 11 Plastic strain increment direction during the loading process.

367

368   The stress-dilatancy relationship actually reflects the variation rules of the plastic strain

369 increment direction. The stress-dilatancy relationship d-χ at different values of β is shown in Fig.

370 12. φ_c=30° is used for demonstration. The model parameters N and μ correspond to β=0.1, 0.4, 0.7

14

371 and 1.0 are listed in Tab. 2. Once the material parameters φ_c and β are obtained, the one-to-one

372 model parameters N and μ can be determined by methods in the following section 3.3.3. For $\beta=1$, N

373 and F equal to M, μ degenerates to 1 and the d-χ relationship is the same with the stress-dilatancy

374 relationship of MCC model. With the decrease of β, the determined values of N and μ decrease

375 accordingly as listed in Tab. 2, and the d-χ relationship curves decline with the decreasing β.

376 Different levels of stress-dilatancy under compression and extension conditions can be reflected as

377 shown in Fig. 12(b), which benefits from the characteristic stress. The difference degree of the

378 stress-dilatancy under triaxial compression and extension conditions enlarges with the decreasing β.

379 Fig. 13 shows the stress-dilatancy curves in the characteristic stress space and the general stress

380 space for $\beta=0.1$. Stress-dilatancy curves at $b=0$, 0.25, 0.5, 0.75 and 1 in the characteristic stress

381 space are coincident, as shown in Fig. 13(a). These coincident curves in the c_{ij} space correspond to

382 a series of stress-dilatancy curves in the σ_{ij} space, as shown in Fig. 13(b).

383 <center>Tab. 2 Parameters in the characteristic stress spaces</center>

φ_c	β	N	μ
	1.0	1.200	1.000
30°	0.7	1.016	0.807
	0.4	0.769	0.537
	0.1	0.381	0.158

384 (a) (b)

385 Fig. 12 Stress-dilatancy relationship for different β-values: (a) in the c_{ij} space; (b) in the σ_{ij} space.

386 (a) (b)

387 Fig. 13 Stress-dilatancy curves when $\beta=0.1$: (a) in the c_{ij} space; (b) in the σ_{ij} space.

388

389 *3.2.3 Hardening parameter*

390 Hardening parameter can be used to describe the hardening/softening rule as well as the

391 evolution of the yield surface. Some valuable studies on hardening parameter have been done to

392 describe the strain hardening and softening properties (Yao *et al.*, 2009; Wang *et al.*, 2018), the

393 stress-dilatancy and state-dependency (Li and Dafalias, 2000) and the particle breakage effect (Xiao

394 and Liu, 2017) et al.. Similar with the MCC model, the plastic volumetric strain is chosen as the

395 hardening parameter in this paper, which can be derived from the linear relationship between e and

lnp for normally consolidated clay under isotropic compression conditions ($\sigma_1 = \sigma_2 = \sigma_3$). As shown in

Fig. 14, the relationship between the void ratio e and $\ln c_{\mathrm{n}}$ can be easily obtained from the linear

relationship of $e \sim \ln p$ under the isotropic compression conditions. Corresponding to the compression

index λ and the swelling index κ in the general stress space, the compression index and the swelling

index in the characteristic stress space become λ/β and κ/β.

<center>Fig. 14 e-$\ln c_{\mathrm{n}}$ relationship in the c_{ij} space.</center>

The way to derive the relationship between the plastic volumetric strain $\varepsilon_{\mathrm{v}}^{\mathrm{p}}$ and the equivalent

consolidation pressure c_{nx} in the c_{ij} space is listed in Tab. 3. The equivalent consolidation pressure

can be written as follows:

$$c_{\mathrm{nx}} = c_{\mathrm{n0}} \exp\left(\frac{\varepsilon_{\mathrm{v}}^{\mathrm{p}}}{\rho_{\mathrm{p}}}\right) \tag{26}$$

where $\rho_{\mathrm{p}} = (\lambda-\kappa)/\beta/(1+e_0)$. e_0 is the initial void ratio. c_{n0} is the initial mean characteristic stress.

<center>Tab. 3 Rule of the strain hardening for clay in the characteristic stress space</center>

	Characteristic stress space
Initial mean characteristic stress	$c_{\mathrm{n0}} = p_0^{\beta}$
Void ratio e	$\Delta e = e - e_0 = -\dfrac{\lambda}{\beta} \ln \dfrac{c_{\mathrm{nx}}}{c_{\mathrm{n0}}}$
volumetric strain ε_{v}	$\varepsilon_{\mathrm{v}} = \dfrac{-\Delta e}{1+e_0} = \dfrac{\lambda}{\beta(1+e_0)} \ln \dfrac{c_{\mathrm{nx}}}{c_{n0}}$
Elastic volumetric strain $\varepsilon_{\mathrm{v}}^{\mathrm{e}}$	$\varepsilon_{\mathrm{v}}^{\mathrm{e}} = \dfrac{-\Delta e^{\mathrm{e}}}{1+e_0} = \dfrac{\kappa}{\beta(1+e_0)} \ln \dfrac{c_{\mathrm{nx}}}{c_{\mathrm{n0}}}$
Plastic volumetric strain $\varepsilon_{\mathrm{v}}^{\mathrm{p}}$	$\varepsilon_{\mathrm{v}}^{\mathrm{p}} = \varepsilon_{\mathrm{v}} - \varepsilon_{\mathrm{v}}^{\mathrm{e}} = \dfrac{\lambda-\kappa}{\beta(1+e_0)} \ln \dfrac{c_{\mathrm{nx}}}{c_{\mathrm{n0}}}$
Equivalent consolidation pressure c_{nx}	$c_{\mathrm{nx}} = c_{\mathrm{n0}} \exp\left(\beta \dfrac{1+e_0}{\lambda-\kappa} \varepsilon_{\mathrm{v}}^{\mathrm{p}}\right) = c_{\mathrm{n0}} \exp\left(\dfrac{\varepsilon_{\mathrm{v}}^{\mathrm{p}}}{\rho_{\mathrm{p}}}\right)$

3.3 Stress-strain relationship

The stress-strain relationship of the normally consolidated clay can be obtained in the c_{ij} space.

<center>16</center>

412 In the elastoplastic theory framework, the total strain increment $d\varepsilon_{ij}$ is divided into the elastic strain

413 increment $d\varepsilon_{ij}^e$ and the plastic strain increment $d\varepsilon_{ij}^p$ as follows:

$$d\varepsilon_{ij} = d\varepsilon_{ij}^e + d\varepsilon_{ij}^p \tag{27}$$

415 *3.3.1 Elastic strain increment*

416   The elastic strain increment can be calculated by the Hook's law.

$$d\varepsilon_{ij}^e = \frac{1+\nu}{E} d\sigma_{ij} - \frac{\nu}{E} d\sigma_{kk}\delta_{ij} \tag{28}$$

418 Based on Eq. (28) and Eq. (16), the elastic principal strain can also be expressed by the characteristic

419 principal stresses as follows:

$$d\varepsilon_1^e = \frac{1}{\beta E} c_1^{\frac{1}{\beta}-1} dc_1 - \frac{\nu}{\beta E}\left(c_2^{\frac{1}{\beta}-1} dc_2 + c_3^{\frac{1}{\beta}-1} dc_3 \right)$$

$$d\varepsilon_2^e = \frac{1}{\beta E} c_2^{\frac{1}{\beta}-1} dc_2 - \frac{\nu}{\beta E}\left(c_3^{\frac{1}{\beta}-1} dc_3 + c_1^{\frac{1}{\beta}-1} dc_1 \right) \tag{29}$$

$$d\varepsilon_3^e = \frac{1}{\beta E} c_3^{\frac{1}{\beta}-1} dc_3 - \frac{\nu}{\beta E}\left(c_1^{\frac{1}{\beta}-1} dc_1 + c_2^{\frac{1}{\beta}-1} dc_2 \right)$$

421 where ν is the Poisson's ratio. The Young's elastic modulus E can be expressed as the function of

422 the mean characteristic stress, as follows:

$$E = 3(1-2\nu)\frac{1+e_0}{\kappa} c_n^{\frac{1}{\beta}} \tag{30}$$

424 *3.3.2 Plastic strain increment*

425   The consistency condition, i.e., the total differential of the yield function Eq. (18), can be

426 expressed as follows:

$$df = \frac{\partial f}{\partial c_n} dc_n + \frac{\partial f}{\partial c_s} dc_s + \frac{\partial f}{\partial c_{nx}} \frac{\partial c_{nx}}{\partial \varepsilon_v^p} d\varepsilon_v^p = 0 \tag{31}$$

428 where $\partial f/\partial c_n = N^2\left(2c_n - c_{nx}\right), \partial f/\partial c_s = 2c_s, \partial f/\partial c_{nx} = -N^2 c_n$. The derivative of c_{nx} with respect

429 to ε_v^p can derived from Eq. (26):

$$\frac{\partial c_{nx}}{\partial \varepsilon_v^p} = \frac{c_{nx}}{\rho_p} \tag{32}$$

431 By substituting $d\varepsilon_v^p$ derived from Eq. (24) together with Eq. (32) into Eq. (31), the plastic

432 multiplier Λ can be derived as follows:

17

433
$$\Lambda = \rho_{\mathrm{p}} \frac{\Gamma(3-\mu)c_{\mathrm{n}}^{\mu}\left[N^2\left(2c_{\mathrm{n}}-c_{\mathrm{nx}}\right)\mathrm{d}c_{\mathrm{n}}+2c_{\mathrm{s}}\mathrm{d}c_{\mathrm{s}}\right]}{N^2 c_{\mathrm{n}}c_{\mathrm{nx}}\left[\mu N^2 c_{\mathrm{n}}^2-(2-\mu)c_{\mathrm{s}}^2\right]}$$
(33)

434   The plastic strain increment is derived by substituting the plastic multiplier Λ in Eq. (33) together

435   with c_{nx} in Eq. (19) into Eq. (24).

436
$$\mathrm{d}\varepsilon_{ij}^{\mathrm{p}} = \rho_{\mathrm{p}}\left[\frac{\delta_{ij}}{3}+\frac{3c_{\mathrm{n}}^{\mu}c_{\mathrm{s}}^{1-\mu}\left(c_{ij}-c_{\mathrm{n}}\delta_{ij}\right)}{\mu N^2 c_{\mathrm{n}}^2-(2-\mu)c_{\mathrm{s}}^2}\right]\frac{\left(N^2 c_{\mathrm{n}}^2-c_{\mathrm{s}}^2\right)\mathrm{d}c_{\mathrm{n}}+2c_{\mathrm{n}}c_{\mathrm{s}}\mathrm{d}c_{\mathrm{s}}}{c_{\mathrm{n}}\left(N^2 c_{\mathrm{n}}^2+c_{\mathrm{s}}^2\right)}$$
(34)

437   The stress-strain relationship in Eq. (34) is totally expressed by the characteristic stresses. It

438   can also degenerate into the MCC model when $\beta=1$. The parameters in Eq. (34) can be determined

439   by the traditional triaxial tests.

3.3.3 Parameters in the proposed model

441   There are only five independent material parameters included in the proposed fractional

442   elastoplastic model, including λ, κ, v, φ_{c} and β, each of which has clear physical significance. Among

443   them, λ, κ, v and φ_{c} are the same as the material parameters included in the MCC model. Only one

444   material parameter β is added, which can be determined by combining φ_{c} for $b=0$ with an additional

445   internal friction angle φ_b for $b\neq0$. According to the critical stress ratio F in the c_{ij} space, which is

446   independent of the b-value, the equation $F|_{b=0}=F|_b$ can be used to determine β.

447
$$\frac{\sqrt{2}\left(R_{\mathrm{c}}^{\beta}-1\right)}{R_{\mathrm{c}}^{\beta}+2} = \frac{\sqrt{\left[R_b^{\beta}-\left(bR_b-b+1\right)^{\beta}\right]^2+\left[\left(bR_b-b+1\right)^{\beta}-1\right]^2+\left(R_b^{\beta}-1\right)^2}}{\left(bR_b-b+1\right)^{\beta}+R_b^{\beta}+1}$$
(35)

448   where $R_{\mathrm{c}}=(1+\sin\varphi_{\mathrm{c}})/(1-\sin\varphi_{\mathrm{c}})$ and $R_b=(1+\sin\varphi_b)/(1-\sin\varphi_b)$. Especially, β can be determined with the

449   internal friction angle φ_{e} for $b=1$ by the following equation (Lu *et al.*, 2017).

450
$$\frac{\left(1+\sin\varphi_{\mathrm{c}}\right)^{\beta}-\left(1-\sin\varphi_{\mathrm{c}}\right)^{\beta}}{\left(1+\sin\varphi_{\mathrm{c}}\right)^{\beta}+2\left(1-\sin\varphi_{\mathrm{c}}\right)^{\beta}} = \frac{\left(1+\sin\varphi_{\mathrm{e}}\right)^{\beta}-\left(1-\sin\varphi_{\mathrm{e}}\right)^{\beta}}{2\left(1+\sin\varphi_{\mathrm{e}}\right)^{\beta}+\left(1-\sin\varphi_{\mathrm{e}}\right)^{\beta}}$$
(36)

451   Thus, β actually reflects the proportional relation of φ_{c} and φ_{e}.

452   In addition, two model parameters, i.e., N and μ, are include in the proposed model, which can

453   be determined by material parameters without the need for additional tests. The determined methods

454   of the model parameters are given as follows:

455   Under the triaxial compression condition with p=constant, $\varepsilon_{\mathrm{v}}^{\mathrm{e}}=0$. Therefore, $\varepsilon_{\mathrm{v}}=\varepsilon_{\mathrm{v}}^{\mathrm{p}}$. When

456   the soil is loaded to the critical state, the variation of the void ratio equals to the vertical distance

457   between the NCL and the CSL, and can be expressed as $\ln2\cdot(\lambda-\kappa)$ (Yu, 1998). Thus, $\varepsilon_{\mathrm{v}}^{\mathrm{p}}$ can be

458   calculated by the following equation:

$$\varepsilon_{\mathrm{v}}^{\mathrm{p}} = \frac{e_0 - e}{1 + e_0} = \frac{\ln 2 \cdot (\lambda - \kappa)}{1 + e_0} \tag{37}$$

460   Therefore, $c_{\mathrm{n}x}$ can be derived by substituting Eq. (37) into Eq. (26):

$$c_{\mathrm{n}x} = c_{\mathrm{n}0} \exp\left(\varepsilon_{\mathrm{v}}^{\mathrm{p}} / \rho_{\mathrm{p}}\right) = 2^{\beta} c_{\mathrm{n}0} \tag{38}$$

462   The critical principal stress $\sigma_{1z} = p_0(1 + 2M/3)$ and $\sigma_{3z} = p_0(1 - M/3)$. The critical mean characteristic

463   stress $c_{\mathrm{n}z} = (\sigma_{1z}^{\beta} + 2\sigma_{3z}^{\beta})/3$ is thus obtained. By substituting the critical stress state $(c_{\mathrm{n}z}, c_{\mathrm{S}z}) = (c_{\mathrm{n}z}, F \cdot c_{\mathrm{n}z})$

464   into Eq. (19), the equivalent consolidation pressure is:

$$c_{\mathrm{n}x} = c_{\mathrm{n}z}\left(F^2 / N^2 + 1\right) \tag{39}$$

466   Combining Eq. (38) with (39), one can get N as follows:

$$N = \sqrt{\frac{F^2 c_{\mathrm{n}z}}{2^{\beta} c_{\mathrm{n}0} - c_{\mathrm{n}z}}} = \sqrt{\frac{F^2\left[(1 + 2M/3)^{\beta} + 2(1 - M/3)^{\beta}\right]}{3 \cdot 2^{\beta} - \left[(1 + 2M/3)^{\beta} + 2(1 - M/3)^{\beta}\right]}} \tag{40}$$

468   where F can be calculated by φ_{c} and β, and M is the function of φ_{c}, as listed in Tab. 1. Therefore, N

469   is actually determined only by φ_{c} and β.

470   When the critical state condition is reached, χ reaches F, and d in Eq. (25) equals 0. The

471   fractional order μ can thus be determined by Eq. (25) as follows:

$$\mu = \frac{2F^2}{N^2 - F^2} \tag{41}$$

473   The fractional order μ is also determined by two material parameters, φ_{c} and β.

474   **3.4 Critical state**

475   The ultimate condition that plastic shearing continues indefinitely without changes in volume

476   and effective stresses has been known as the critical state (Muir Wood, 1990). It has been testified

477   that the critical state is closely related to the true 3D stress conditions and should be reflected in

478   constitutive models (Zhao and Guo, 2013; Xiao and Liu, 2017; Zhou *et al.*, 2017), which can be

479   reflected by the characteristic stress in the proposed fractional elastoplastic model.

480   The soil parameters for Fujinomori clay, which are stated in section 4.1, are used to exhibit the

481   critical state properties that reflected by the proposed model. The stress paths of $b=0$, $b=0.5$ and $b=1$

482   when p=constant under the drained condition and the undrained condition ($\varepsilon_{\mathrm{v}}=0$) are shown in the

483   c_{ij} space in Fig. 15(a) and the σ_{ij} space in Fig. 15(b), respectively. Stress paths of $b=0$, $b=0.5$ and

484 $b=1$ in the c_{ij} space are different but reach to a unique critical state line, which correspond to different

485 stress paths and different CSLs in the σ_{ij} space. That is, the critical state is reached when χ equals to

486 F. At the same time, η reaches the critical stress ratio M_b for a certain value of b in the σ_{ij} space. The

487 critical state behaviour of soils under true 3D stress conditions is thus reflected by the unique critical

488 state line in the c_{ij} space.

489

490   (a)   (b)

491   Fig. 15 Stress paths and critical state lines: (a) in the c_{ij} space; (b) in the σ_{ij} space.

492

4 Experimental verification

494   The existing fractional models for soil cannot describe the deformation properties of soils under

495 the true 3D stress conditions. The capability of the proposed fractional elastoplastic model in

496 capturing the deformation properties of soil is thus examined by predicting test results and

497 comparing with the predictions of the MCC model. The true triaxial test results of the new

498 Fujinomori (NF) clay under the drained conditions (Chowdhury and Nakai, 1998) and the Grundite

499 clay under the undrained conditions (Lade and Musante, 1978) are used in this paper.

4.1 Fujinomori clay

501   Drained true triaxial tests were performed on the normally consolidated NF clay at a constant

502 mean stress $p=196$kPa. The values of the intermediate principal stress coefficient b were set as 0,

503 0.268, 0.5 and 0.732, corresponding to different stress Lode angles $\theta=0°$, 15°, 30°, 45°, respectively.

504 The values of material parameters for the NF clay used in the models are $\varphi_c=33.7°$, $\lambda/(1+e_0)=0.0508$,

505 $\kappa/(1+e_0)=0.0112$ and $v=0.3$. The characteristic material parameter $\beta=0.1$ is used for predictions.

506 Accordingly, the model parameters $N=0.4248$ and $\mu=0.1654$ are determined by Eqs. (40) and (41).

507   The experimental data from Chowdhury and Nakai (1998) are arranged in terms of the relation

508 among principal stress ratio σ_1/σ_3, volumetric strain ε_v and principal strains (ε_1, ε_2 and ε_3), as

509 indicated by the open circles in Fig. 16. These true triaxial test data at different b-values are predicted

510 by the proposed 3D fractional elastoplastic model and the MCC model, which are indicated by the

511 red solid line and the black dash line, respectively. Both the proposed model and the MCC model

512 can well predict the stress-strain behaviour under triaxial compressions conditions, i.e., $b=0$, as

513 shown in Fig. 16(a). However, for $b=0.268$, 0.5 and 0.732, the experimental stress-strain behaviour

20

514 is predicted by the proposed fractional model better than the MCC model, as shown in Fig. 16(b)~(d).

515 That is, the proposed fractional elastoplastic model can well capture the strength property and the

516 deformation behaviour of the normally consolidated NF clay under the drained triaxial conditions.

517

518   (a)   (b)   (c)   (d)

519   Fig. 16 Comparison between test results (data from Chowdhury and Nakai, 1998) and predicted results

520   under true 3D stress conditions at p=196kPa with: (a) b=0; (b) b=0.268; (c) b=0.5; (d) b=0.732.

521

522   The relationship between the strains under true 3D stress conditions is actually a reflection of

523   the deformation flow direction of soil. Test results with different b-values are arranged in terms of

524   the relation between ε_2 and ε_1 and the relation between ε_3 and ε_1, as shown by dots in Fig. 17. Test

525   results shown in Fig. 17(a) indicate that ε_2 is negative, i.e., extensive, when b=0 and b=0.268, and

526   is positive, i.e., compressive, when b=0.5 and b=0.732. Fig. 17(b) shows that ε_3 is extensive in all

527   the cases, and the extent of extensive gradually decreases for higher b-values. The experimental

528   relation between ε_2 and ε_1 and between ε_3 and ε_1 for a constant b-value, as well as the variation rule

529   for different b-values, are all reasonably captured by the proposed fractional model better than the

530   MCC model.

531

532   (a)   (b)

533   Fig. 17 Comparisons between test results (data from Chowdhury and Nakai, 1998) and predicted

534   results between principal stains: (a)ε_2-ε_1; (a) ε_3-ε_1.

535

536   **4.2   Grundite clay**

537   Undrained true triaxial experimental study was performed by Lade and Musante (1978) to

538   study the influence of b on the stress-strain behaviour, pore pressure and strength properties of

539   normally consolidated Grundite clay. Cubical specimens of the remolded Grundite clay were tested

540   at a consolidation pressure of σ_c=147kPa and all three principal stresses are independently controlled.

541   b was maintained constant in each test, and b=0.00, 0.21, 0.40, 0.70 and 0.95, separately. Soil

542   parameters for predictions are from Yao et $al.$ (2004) and listed as: φ_c=28.2°, $\lambda/(1+e_0)$=0.0846,

543   $\kappa/(1+e_0)$=0.0169 and v=0.27. φ_e=31.18° from the test with b=0.95 is used to determine β=0.303.

544   Correspondingly, the model parameters $N=0.6289$ and $\mu=0.4222$ are determined from Eqs. (40) and

545   (41).

546   Fig. 18 shows the comparison between test data and predicted lines presented in terms of

547   relations among the principal stress ratio σ_1/σ_3, the pore pressure ratio u/σ_c and the principal strain

548   ε_1, separately. When $b=0$, the predicted lines of the proposed fractional elastoplastic model are

549   almost the same with the predicted lines of the MCC model, and they both capture the experimental

550   stress-strain behaviour well, as shown in Fig. 18(a). The shear strengths of the Grundite clay with

551    $b=0.21$, 0.40, 0.70 and 0.95 are well captured by the proposed model, but obviously overpredicted

552   by the MCC model, as shown in Fig. 18(b)-(d). In addition, the proposed fractional elastoplastic

553   model better predicts the relationship between u/σ_c and ε_1 for $b\neq0$ than the MCC model.

554

555   (a)   (b)   (c)   (d)   (e)

556   Fig. 18 Comparisons between test results (data from Lade and Musante, 1978) and predicted results

557   with $\sigma_c=147$ kPa and: (a) $b=0$; (b) $b=0.21$; (b) $b=0.40$; (d) $b=0.70$; (e) $b=0.95$.

558

559   The test data between principal strains under undrained conditions are compared with the

560   predicted lines of the proposed fractional elastoplastic model and the MCC model. Test results are

561   represented by dots. The predictions of the proposed model and the MCC model are represented by

562   the red solid lines and the black dash lines, respectively. The test results and the predictions of ε_2

563   and ε_3 are plotted versus ε_1 for different b-values, as shown in Fig. 19. As shown in Fig. 19(a), ε_2

564   changes from extension to compression as b increases. ε_3 is under extension for all b-values, and the

565   extent of extension gradually decreases with a larger b-value, as shown in Fig. 19(b). By comparison,

566   the ability of the proposed model to capture the relationship between the principal strains under true

567   3D stress conditions is demonstrated to be better than the MCC model.

568

569   (a)   (b)

570   Fig. 19 Comparisons between test results (data from Lade and Musante, 1978) and predicted results

571   between principal stains: (a) ε_2-ε_1; (b) ε_3-ε_1.

572

573 **5   Conclusions**

574   In the present study, a novel 3D fractional plastic flow rule without limiting the coordinate

575   basis of the differentiable function was proposed, which is in coordination with the framework of

576   the elastoplastic theory. The plastic strain increment direction for soil under the true 3D stress

577   conditions can be determined in two steps: firstly, determine the direction in an interim coordinate

578   system, and then transform it into general stress space. The 3D fractional plastic flow rule offers a

579   possibility to develop a fractional elastoplastic model for geomaterials, like soils, concretes and

580   rocks, even for the hydrostatic pressure independent materials, like metallic materials.

581   In the characteristic stress space, by combining the proposed fractional plastic flow rule with

582   the ellipsoidal yield function, and further taking the plastic volumetric strain as the hardening

583   parameter, a 3D fractional elastoplastic constitutive model for soil was proposed for the first time.

584   The proposed model has only one more material parameter, i.e. β, than the MCC model. It can well

585   reflect the variation rule of the plastic strain increment direction under complex loading conditions

586   and the properties of the critical state for soil. The comparison between the model predictions and

587   the test results indicates that the proposed model can properly capture the strength and deformation

588   behaviour of soils under true 3D stress conditions.

594

595

596

597

598

599   **List of notations**

        E Young's elastic modulus

        F critical characteristic stress ratio

        M failure stress ratio

N	ratio of the vertical axis and the horizontal axis of the yield curve
Q_{ij}	orthogonal tensor for transformation
R_b	principal stress ratio under constant b
R_c	principal stress ratio under triaxial compression conditions
S_{kl}, S_k	interim stress tensor and its eigenvalue
I_1, I_2, I_3	first, second and third stress invariants
b	intermediate principal stress coefficient
c_{ij}	characteristic stress tensor
c_i	characteristic principal stress
c_n, c_s	mean characteristic stress and characteristic deviatoric stress
c_{n0}	initial mean characteristic stress
d	stress-dilatancy ratio
e, e_0	void ratio and its initial value
l_i^j	covariant transformation coefficient
p, q, θ	mean stress, deviatoric stress and stress Lode angle
p_0	initial mean stress
p_r	reference stress for dimensionless transformation
$m_{ij}^{(\sigma)}, m_{kl}^{(S)}$	components of the fractional gradient vector of f in the σ_{ij} space and in the S_{kl} space
$n_{ij}^{(\sigma)}, n_{kl}^{(S)}$	components of the gradient vector of g in the σ_{ij} space and in the S_{kl} space
$\mathbf{m}_{\mathbf{m}\mu}, \mathbf{m}_{\mathbf{d}\mu}$	components of the fractional gradient vector of f
$\mathbf{n}_{\mathbf{m}g}, \mathbf{n}_{\mathbf{d}g}$	components of the gradient vector of g
$\Gamma(\cdot)$	Euler Gamma function
Λ	plastic multiplier for fractional plastic flow rule
$d\lambda$	plastic multiplier for classical plastic flow rule

β	characteristic stress index	
δ_{ij}	Kronker delta tensor	
$\varepsilon_{ij}, \varepsilon_{ij}^{e}, \varepsilon_{ij}^{p}$	strain tensor, elastic strain tensor and plastic strain tensor	
$\varepsilon_{v}, \varepsilon_{v}^{e}, \varepsilon_{v}^{p}$	volumetric strain, elastic volumetric strain and plastic volumetric strain	
ε_{s}^{p}	deviatoric plastic strain related to q	
ε_{θ}^{p}	deviatoric plastic strain related to θ	
η	stress ratio	
κ	swelling index	
λ	compression index	
μ	fractional order	
v	Poisson's ratio	
σ_{i}	principal stress	
σ_{ij}	stress tensor	
φ	internal friction angle	
χ	characteristic stress ratio	

600

601

602

603

604

605

606 **Figures**

607

608

609 (a)

610

611 (b)
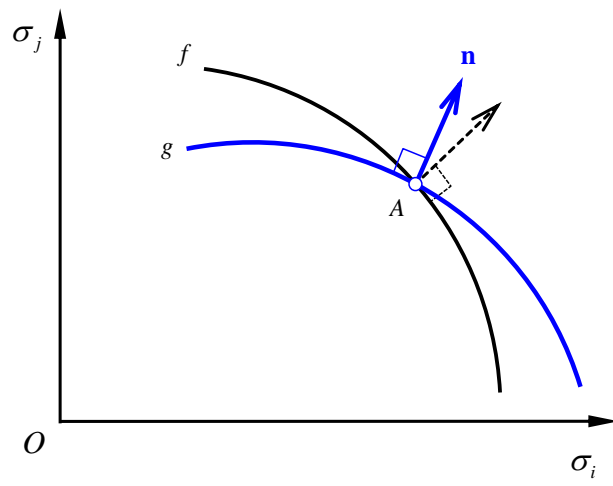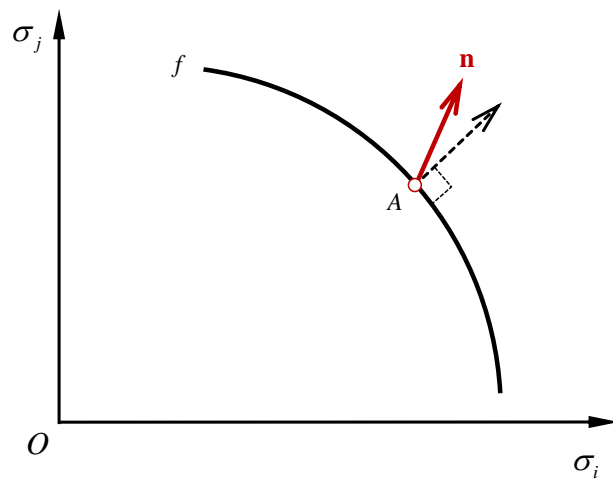
612 Fig. 1 Two ways to determine the plastic flow direction:

613 (a) orthogonal way; (b) non-orthogonal way.
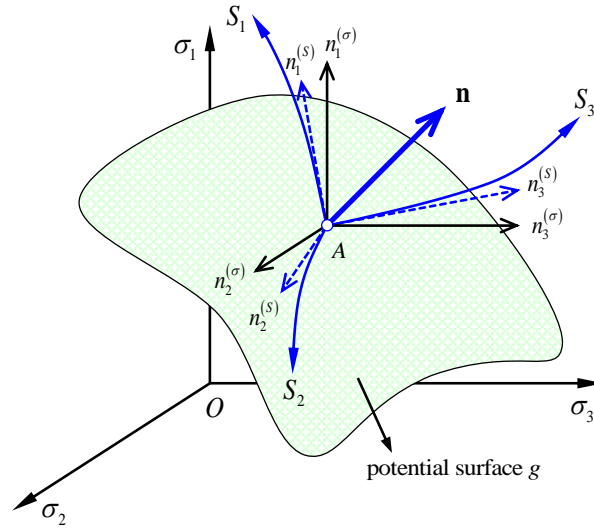
Fig. 2 Coordinate transformation of the plastic flow direction.

616

617   (a)

618

619   (b)
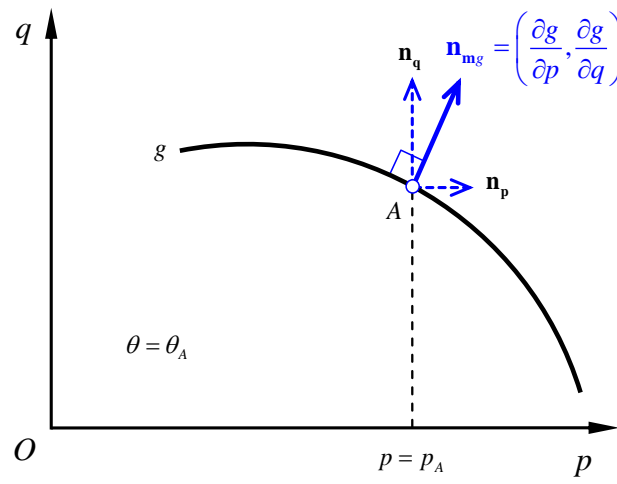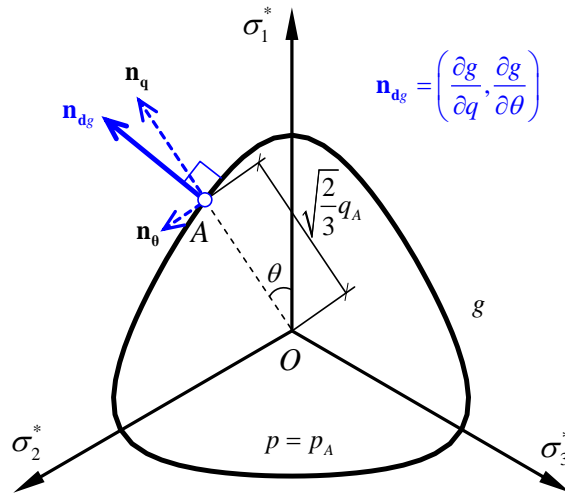
620   Fig. 3 Plastic flow direction in: (a) the meridian plane with $\theta=\theta_A$; (b) the deviatoric plane with $p=p_A$.

621

622

623   (a)   (b)

624
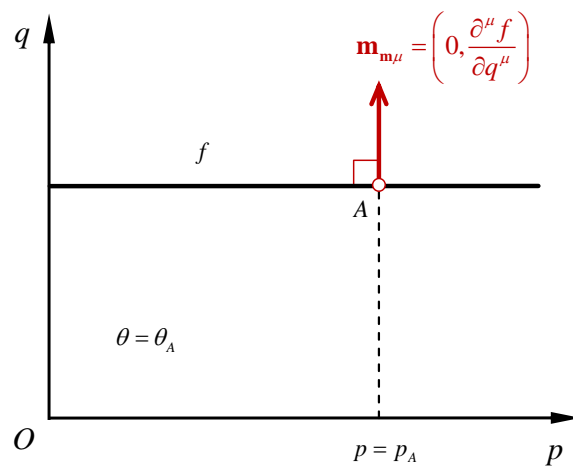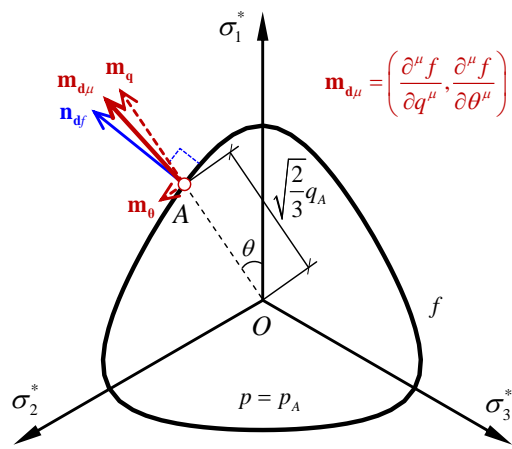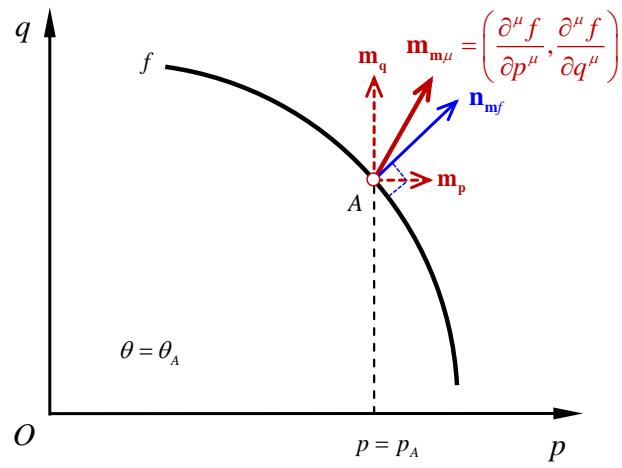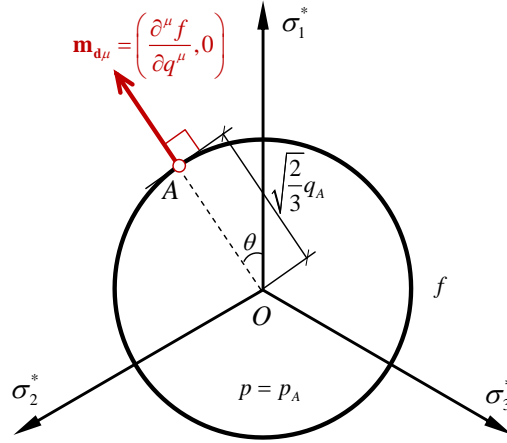
(c)   (d)

Fig. 4 Fractional plastic flow direction with the yield function constructed:

(a) by p, q and θ in the meridian plane; (b) by p, q and θ in the deviatoric plane;

(c) only by q and θ in the meridian plane; (d) only by p and q in the deviatoric plane.
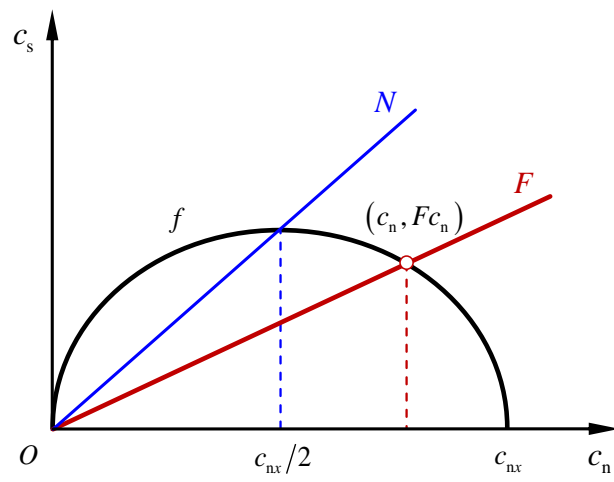
630

631

Fig. 5 Yield surface in the meridian plane

632

(a)

634

635

(b)
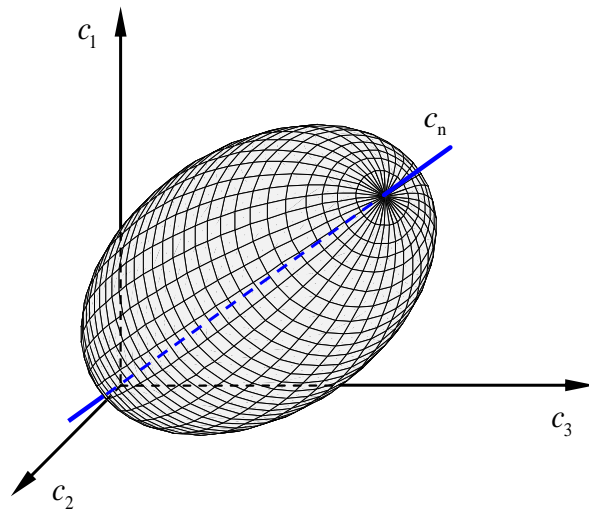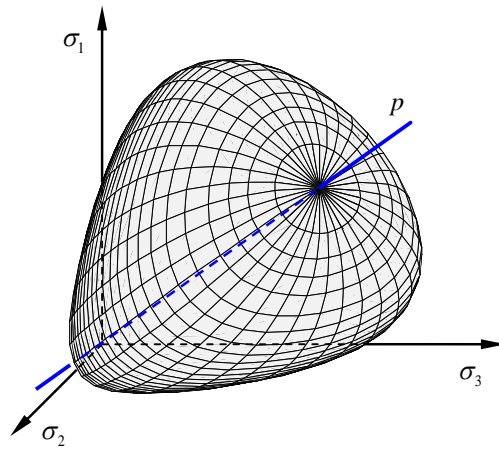
636   Fig. 6 Yield surface: (a) in the c_{ij} space; (b) in the σ_{ij} space.

(a)

(b)

Fig. 7 Yield curves in the σ_{ij} space with the decrease of β:

(a) in the meridian plane; (b) in the deviatoric plane.

643

(a)

645

646

(b)

647   Fig. 8 Yield curve in the σ_{ij} space with the increase of q at a constant p:

648   (a) in the meridian plane; (b) in the deviatoric plane.

649

650

(a)

651

652

(b)
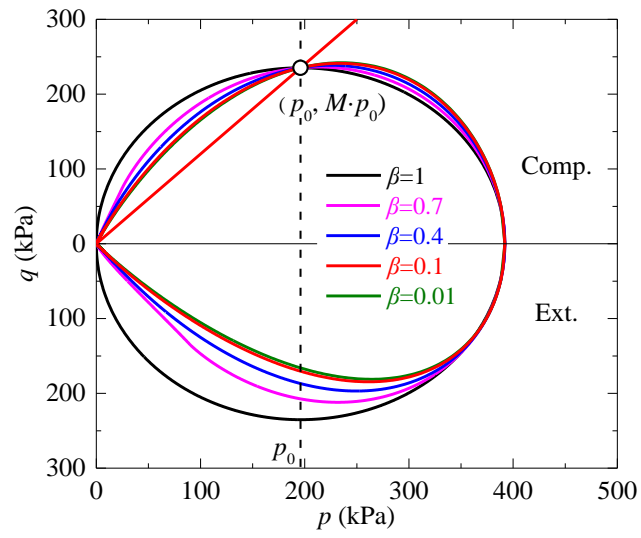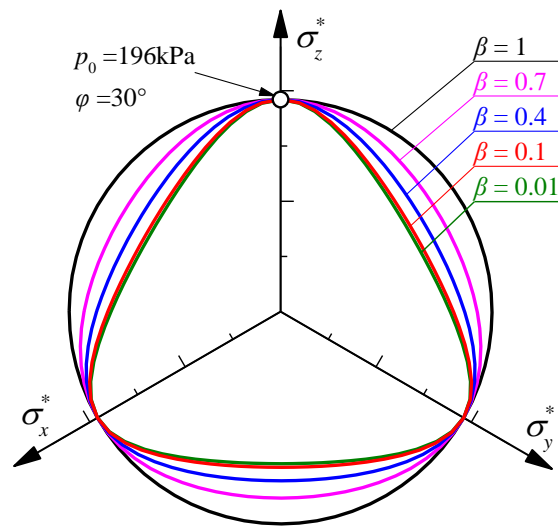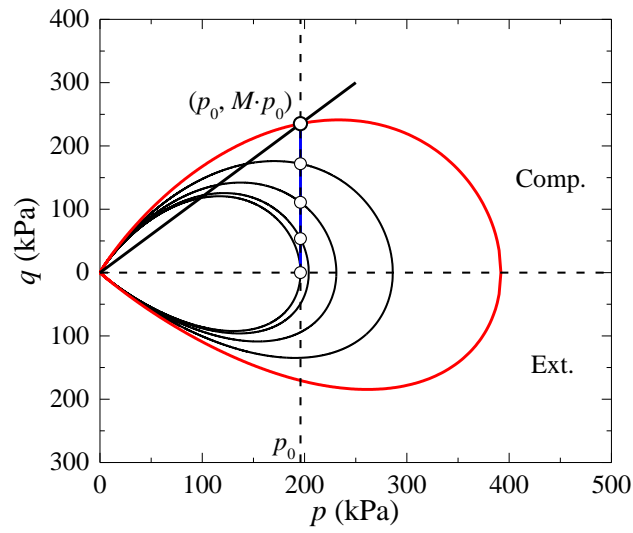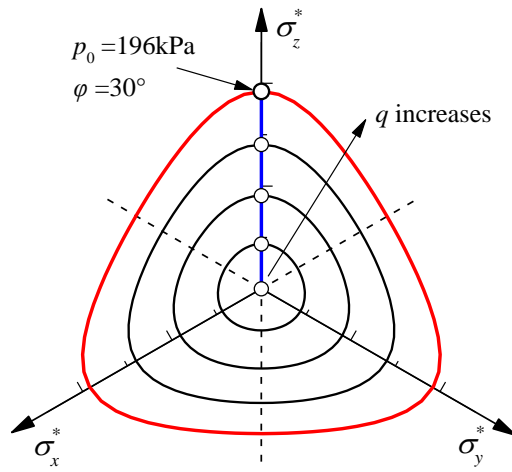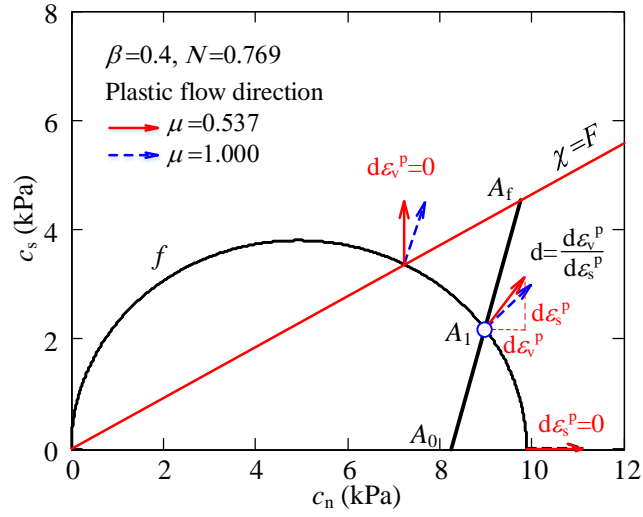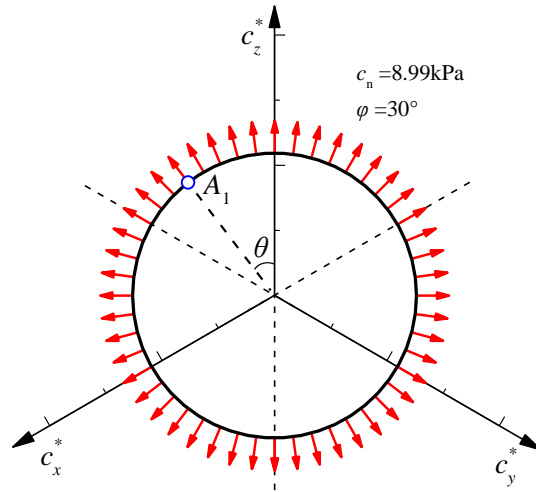
653 Fig. 9 Plastic flow direction in the c_{ij} space at the current loading point:

654 (a) in the meridian plane with $\theta=\theta_A$; (b) in the deviatoric plane with $p=p_A$.

655
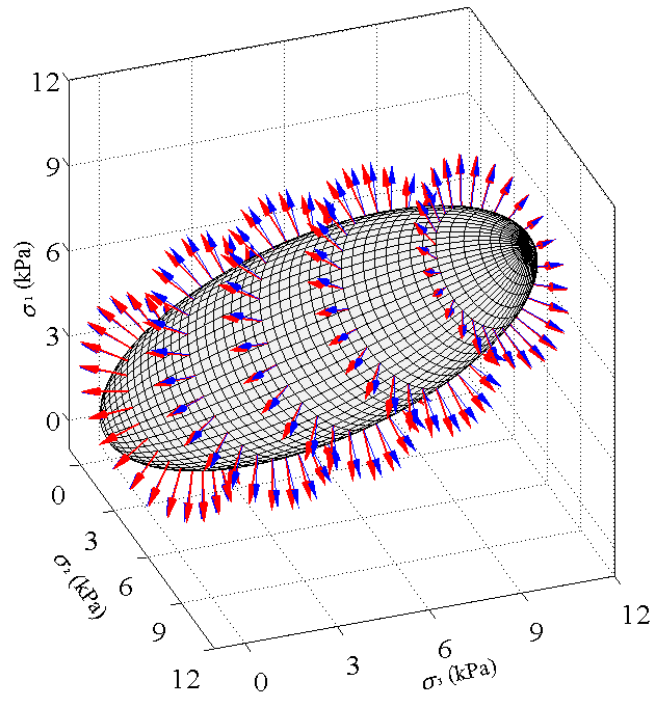
656 Fig. 10 Plastic flow direction in the c_{ij} space.

657
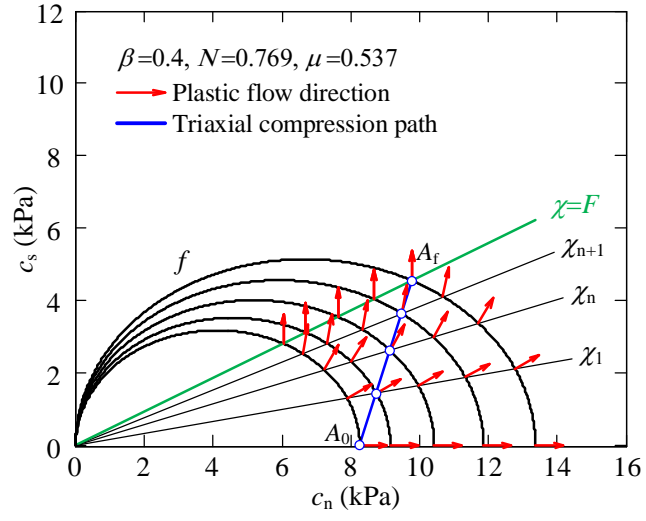
658   Fig. 11 Plastic flow direction during the loading process.
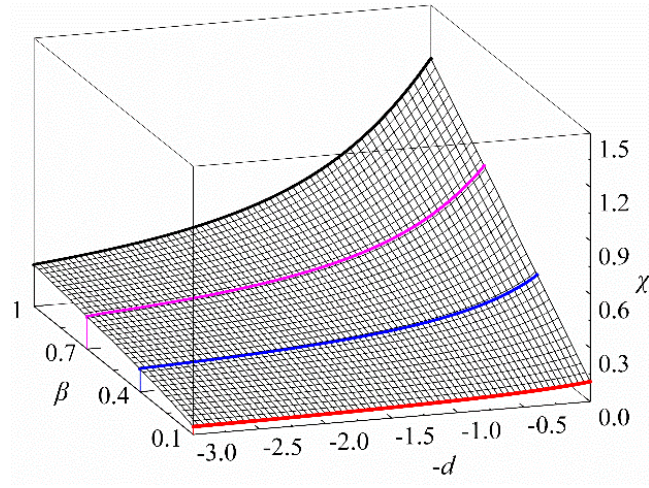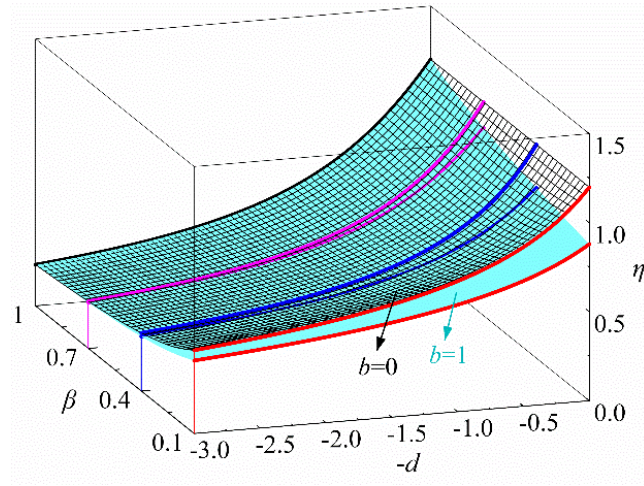
659

660 (a)

661

662 (b)

663　　　Fig. 12 Stress-dilatancy relationship for different β-values: (a) in the c_{ij} space; (b) in the σ_{ij} space.

664

665 (a)

666

667 (b)
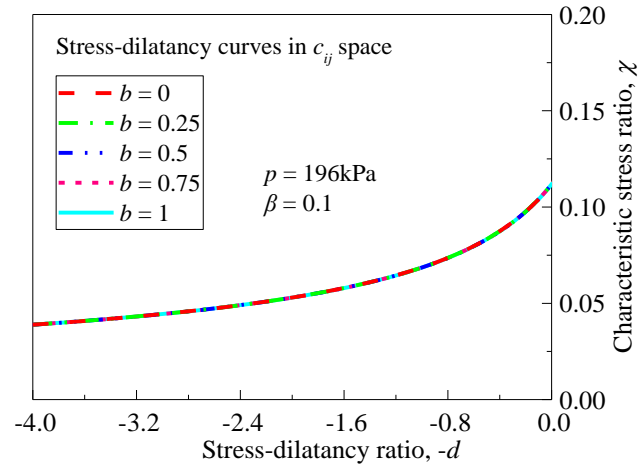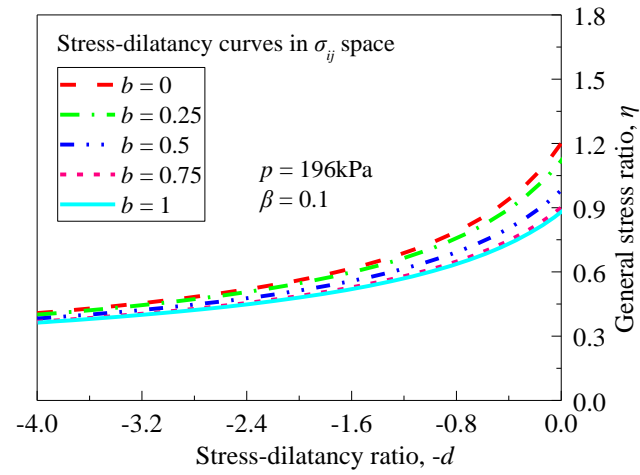
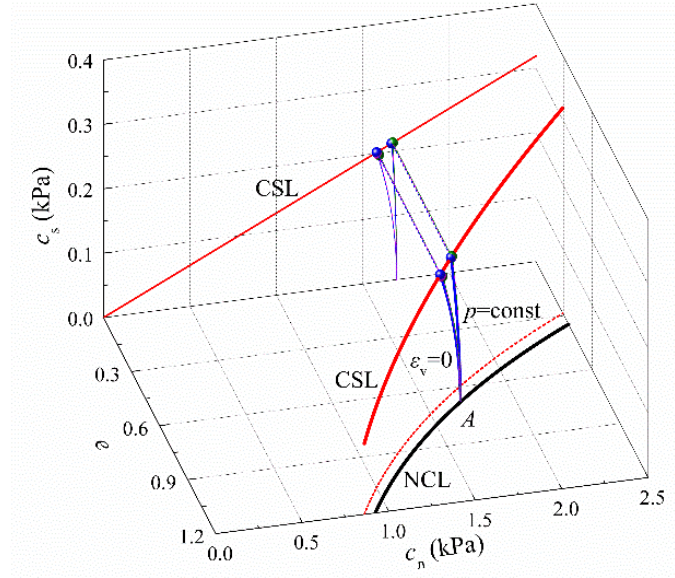668 Fig. 13 Stress-dilatancy curves when β=0.1: (a) in the c_{ij} space; (b) in the σ_{ij} space.

669
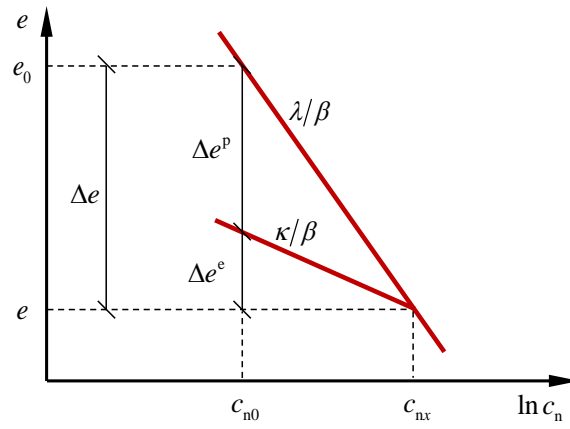
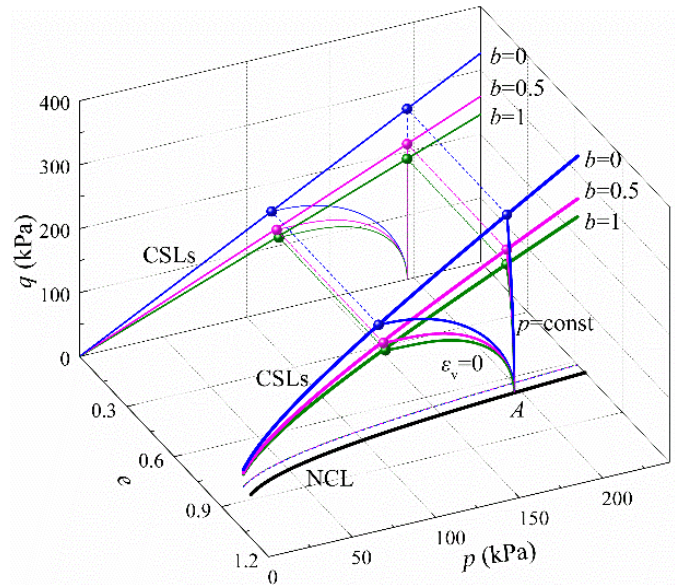670

671　Fig. 14 e-$\ln c_n$ relationship in the c_{ij} space.

672

673   (a)

674

675   (b)

676   Fig. 15 Stress paths and critical state lines: (a) in the c_{ij} space; (b) in the σ_{ij} space.

677
678   (a)   (b)

679
680   (c)   (d)
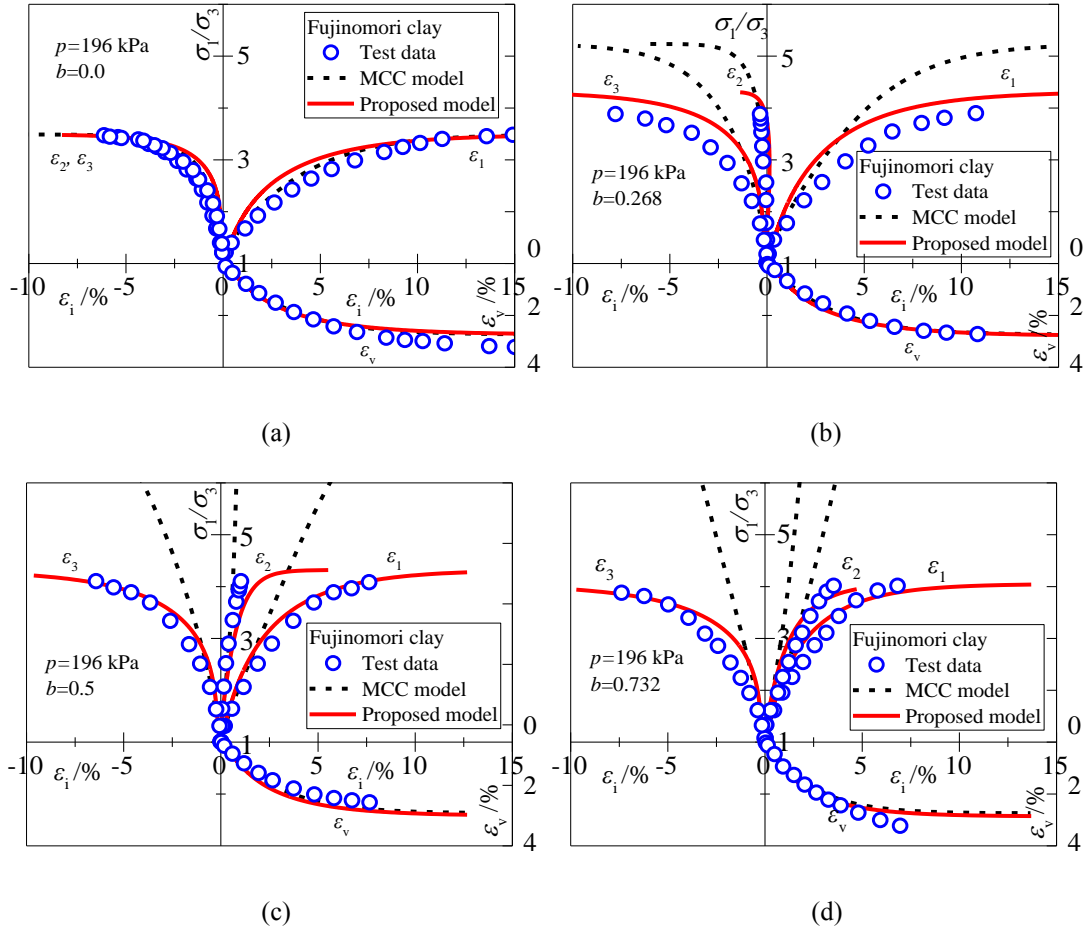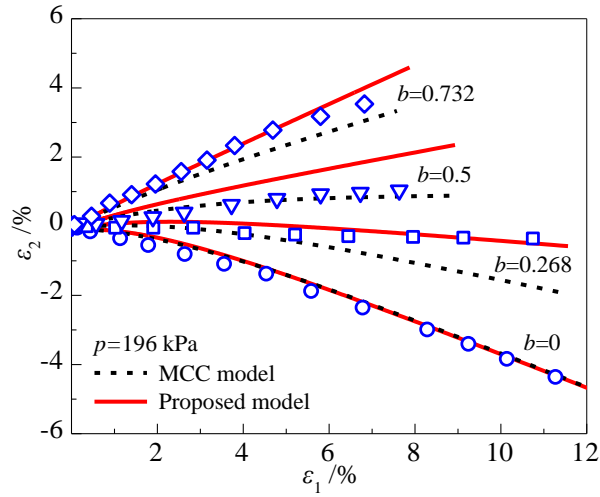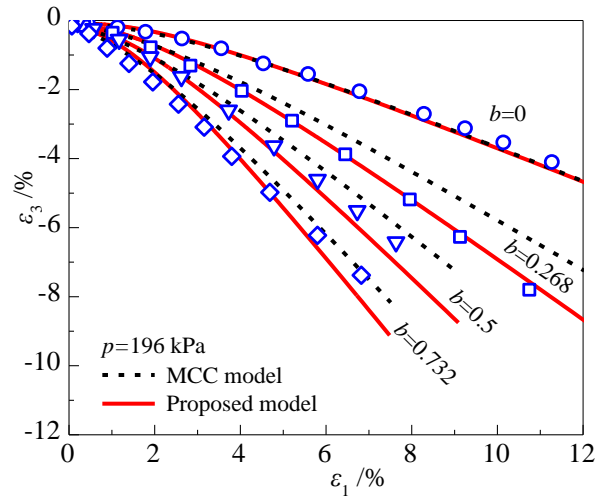
681   Fig. 16 Comparison between test results (data from Chowdhury & Nakai, 1998) and predicted results

682   under true 3D stress conditions at p=196kPa with: (a) b=0; (b) b=0.268; (c) b=0.5; (d) b=0.732.

683

684   (a)

685

686   (b)

687   Fig. 17 Comparisons between test results (data from Chowdhury & Nakai, 1998) and predicted results

688   between principal stains: (a)ε_2-ε_1; (a) ε_3-ε_1.

689

690   (a)   (b)

691

692   (c)   (d)

693

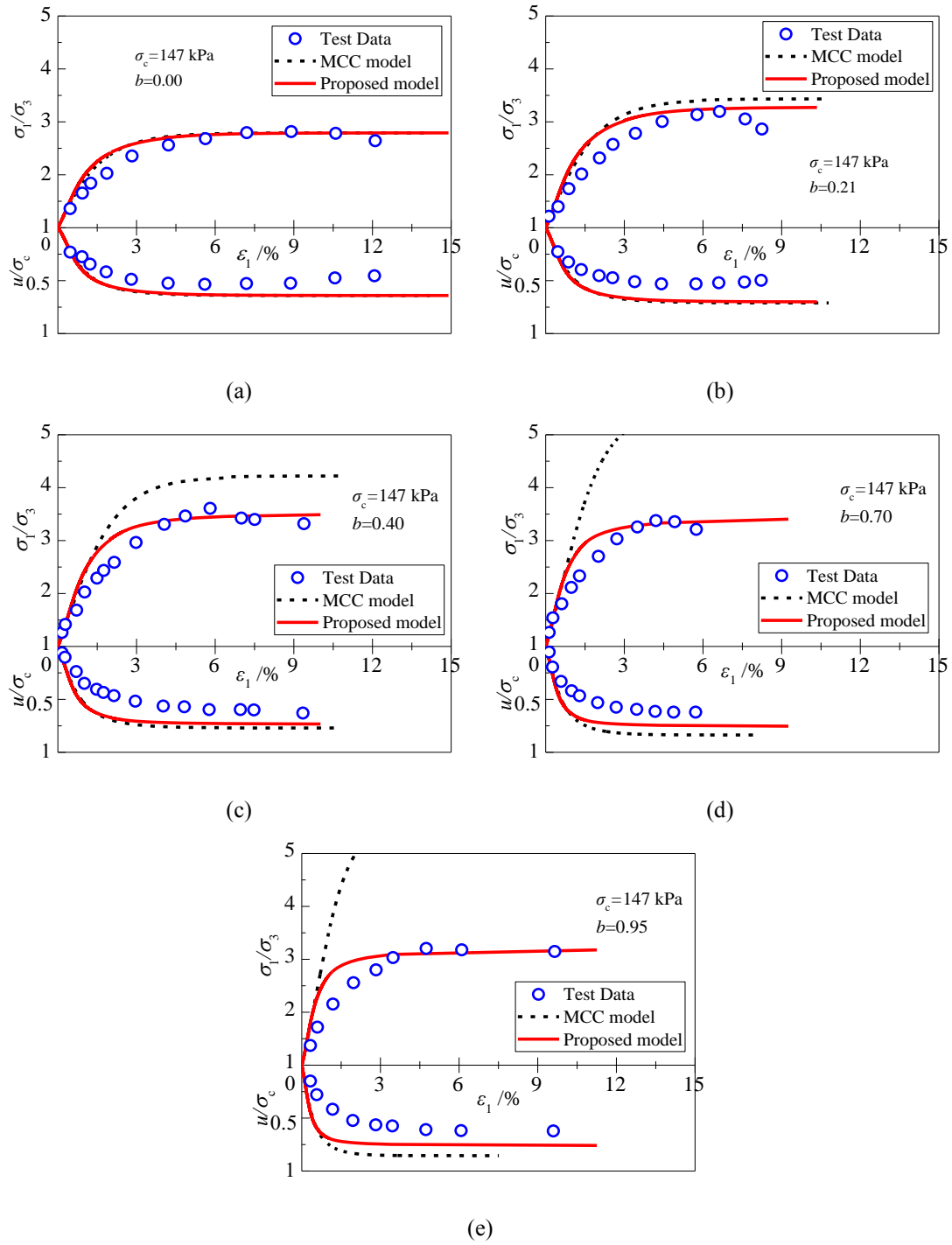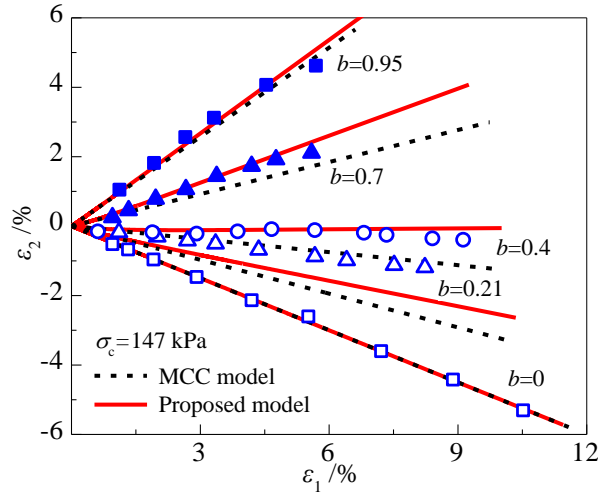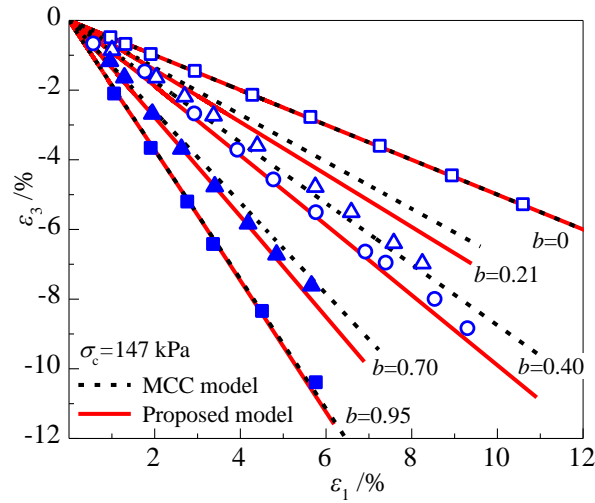694   (e)

695   Fig. 18 Comparisons between test results (data from Lade & Musante, 1978) and predicted results with

696   σ_c=147 kPa and: (a) b=0; (b) b=0.21; (b) b=0.40; (d) b=0.70; (e) b=0.95.

(a)

(b)

Fig. 19 Comparisons between test results (data from Lade & Musante, 1978) and predicted results

between principal stains: (a) ε_2-ε_1; (b) ε_3-ε_1.

REFERENCES

Borja, R. I., Sama, K. M., and Sanz, P. F., 2003. On the numerical integration of three-invariant elastoplastic constitutive models. *Comput. Methods Appl. Mech. Eng.* 192 (9-10), 1227-1258.

Chowdhury, E. Q., and Nakai, T., 1998. Consequences of the t_{ij}-concept and a new modeling approach. *Comput. Geotech.* 23 (3), 131-164.

Colinas-Armijo, N., Paola, M. D., and Pinnola, F. P., 2016. Fractional characteristic times and dissipated energy in fractional linear viscoelasticity. *Commun. Nonlinear Sci.* 37, 14-30.

Collins, I. F., 2003. A systematic procedure for constructing critical state models in three dimensions.

712 *Int. J. Solids Struct.* 40 (17), 4379-4397.

713 Collins, I. F., and Houlsby, G. T., 1997. Application of thermomechanical principles to the modelling of

714 geotechnical materials. *Proceedings of the Royal Society a: Mathematical, Physical and Engineering*

715 *Sciences*. 453 (1964), 1975-2001.

716 Duriez, J., and Vincens, É., 2015. Constitutive modelling of cohesionless soils and interfaces with

717 various internal states: an elasto-plastic approach. *Comput. Geotech.* 63, 33-45.

718 Gao, Z. W., and Zhao, J. D., 2017. A non-coaxial critical-state model for sand accounting for fabric

719 anisotropy and fabric evolution. *Int. J. Solids Struct.* 106-107, 200-212.

720 Khalili, N., and Liu, M. D., 2008. On generalization of constitutive models from two dimensions to three

721 dimensions. *Int. J. Numer. Anal. Met.* 32 (17), 2045-2065.

722 Lade, P. V., and Musante, H. M., 1978. Three-dimensional behavior of remolded clay. *Journal of the*

723 *Geotechnical Engineering Division, ASCE*. 104 (2), 193-209.

724 Lade, P. V., Nelson, R. B., and Ito, Y. M., 1987. Nonassociated flow and stability of granular materials.

725 *J. Eng. Mech, ASCE.* 113 (9), 1302-1318.

726 Li, X. S., and Dafalias, Y. F., 2000. Dilatancy for cohesionless soils. *Géotechnique*. 50 (4), 449-460.

727 Lu, D. C., Liang, J. Y., Du, X. L., Wang, G. S., and Shire, T., 2018. A novel transversely isotropic

728 strength criterion for soils based on a mobilised plane approach. *Géotechnique*,

729 https://doi.org/10.1680/jgeot.17.P.191.

730 Lu, D. C., Ma, C., Du, X. L., Jin, L., and Gong, Q. M., 2017. Development of a new nonlinear unified

731 strength theory for geomaterials based on the characteristic stress concept. *International Journal of*

732 *Geomechanics, ASCE*. 17 (2), 4016058.

733 Lu, D. C., Du, X. L., Wang, G. S., Zhou, A. N., and Li, A. K., 2016. A three-dimensional elastoplastic

734 constitutive model for concrete. *Computers and Structures*. 163, 41-55.

735 Ma, C., Lu, D. C., Du, X. L., and Zhou, A. N., 2017. Developing a 3D elastoplastic constitutive model

736 for soils: a new approach based on characteristic stress. *Comput. Geotech.* 86, 129-140.

737 Mashayekhi, S., Miles, P., Hussaini, M. Y., and Oates, W. S., 2018. Fractional viscoelasticity in fractal

738 and non-fractal media: theory, experimental validation, and uncertainty analysis. *J. Mech. Phys. Solids*.

739 111, 134-156.

740 Meng, R., Yin, D., Zhou, C., and Wu, H., 2016. Fractional description of time-dependent mechanical

741 property evolution in materials with strain softening behavior. *Appl. Math. Model.* 40 (1), 398-406.

742 Mortara, G., 2015. A constitutive framework for the elastoplastic modelling of geomaterials. *Int. J. Solids*

743 *Struct.* 63 (6), 139-152.

744 Muir Wood, D. M., 1990. Soil behaviour and critical state soil mechanics. Cambridge University Press.

745 Nakai, T., Shahin, H. M., Kikumoto, M., Kyokawa, H., Zhang, F., and Farias, M. M., 2011. A simple

746 and unified three-dimensional model to describe various characteristics of soils. *Soils Found.* 51 (6),

747   1149-1168.

748   Panteghini, A., and Lagioia, R., 2018. An extended modified Cam-clay yield surface for arbitrary

749   meridional and deviatoric shapes retaining full convexity and double homothety. *Géotechnique*. 68

750   (7), 590-601.

751   Podlubny, I., 1998. Fractional differential equations: an introduction to fractional derivatives fractional

752   differential equations to methods of their solution and some of their applications. Academic Press.

753   Roscoe, K. H., and Burland, J. B. On the generalised stress-strain behaviour of 'wet' clay. In: Heyman,

754   J., and Leckie, F. A., eidtors. Engineering Plasticity. Cambridge at the University Press; 1968, pp.

755   535-609.

756   Sumelka, W., 2014. Fractional viscoplasticity. *Mech. Res. Commun.* 56, 31-36.

757   Sumelka, W., and Nowak, M., 2016. Non-normality and induced plastic anisotropy under fractional

758   plastic flow rule: a numerical study. *Int. J. Numer. Anal. Met.* 40 (5), 651-675.

759   Sun, D. A., Matsuoka, H., Yao, Y. P., and Ishii, H., 2004. An anisotropic hardening elastoplastic model

760   for clays and sands and its application to FE analysis. *Comput. Geotech.* 31 (1), 37-46.

761   Sun, Y. F., Indraratna, B., Carter, J. P., Marchant, T., and Nimbalkar, S., 2017. Application of fractional

762   calculus in modelling ballast deformation under cyclic loading. *Comput. Geotech.* 82, 16-30.

763   Sun, Y. F., and Xiao, Y., 2017. Fractional order plasticity model for granular soils subjected to monotonic

764   triaxial compression. *Int. J. Solids Struct.* 118-119, 224-234.

765   Sun, Y. F., Gao, Y. F., and Shen, Y., 2018a. Mathematical aspect of the state-dependent stress-dilatancy

766   of granular soil under triaxial loading. *Géotechnique*., https://doi.org/10.1680/jgeot.17.T.029.

767   Sun, Y. F., Gao, Y. F., and Zhu, Q. Z., 2018b. Fractional order plasticity modelling of state-dependent

768   behaviour of granular soils without using plastic potential. *Int. J. Plasticity*. 102 (3), 53-69.

769   Wang, G. S., Lu, D. C., Du, X. L., Zhou, X., and Cao, S. T., 2018. A true 3d frictional hardening

770   elastoplastic constitutive model of concrete based on a unified hardening/softening function. *J. Mech.*

771   *Phys. Solids*. 119, 250-273.

772   Xiao, Y., and Liu, H. L., 2017. Elastoplastic constitutive model for rockfill materials considering particle

773   breakage. *Int. J. Geomech.* 17 (1), 4016041.

774   Xiao, Y., Liu, H. L., Chen, Y. M., and Jiang, J. S., 2004. Bounding surface plasticity model incorporating

775   the state pressure index for rockfill materials. *J. Eng. Mech, ASCE.* 141 (11), 4014087.

776   Yao, Y. P., Hou, W., and Zhou, A. N., 2009. UH model: three-dimensional unified hardening model for

777   overconsolidated clays. *Géotechnique*. 59 (5), 451-469.

778   Yao, Y. P., Lu, D. C., Zhou, A. N., and Zou, B., 2004. Generalized non-linear strength theory and

779   transformed stress space. *Science in China Ser. E*. 47 (6), 691-709.

780   Yu, H. S., 1998. CASM: a unified state parameter model for clay and sand. *Int. J. Numer. Anal. Met.* 22

781   (8), 621-653.

782   Zhao, J. D., and Guo, N., 2013. Unique critical state characteristics in granular media considering fabric

783   anisotropy. *Géotechnique*. 63 (8), 695-704.

784   Zhou, A. N., and Sheng, D. C., 2015. An advanced hydro-mechanical constitutive model for unsaturated

785   soils with different initial densities. *Comput. Geotech.* 63, 46-66.

786   Zhou, W., Liu, J. Y., Ma, G., and Chang, X. L., 2017. Three-dimensional DEM investigation of critical

787   state and dilatancy behaviors of granular materials. *Acta Geotech.* 12 (3), 527-540.